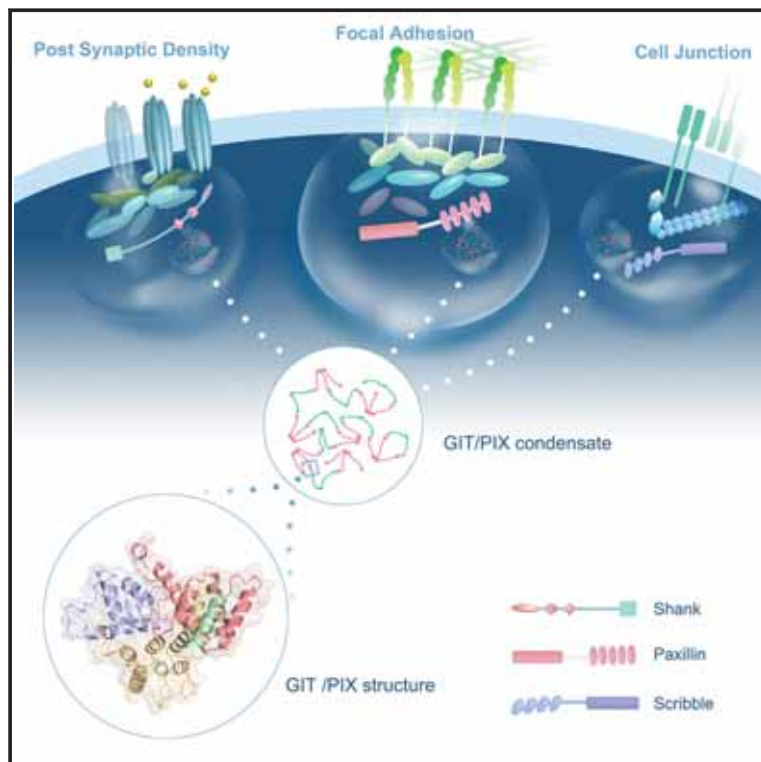


# Molecular Cell

## GIT/PIX Condensates Are Modular and Ideal for Distinct Compartmentalized Cell Signaling

### Graphical Abstract



### Authors

Jinwei Zhu, Qingqing Zhou,  
Yitian Xia, ..., Mengjuan Peng,  
Rongguang Zhang, Mingjie Zhang

### Correspondence

jinwei.zhu@sjtu.edu.cn (J.Z.),  
rgzhang@sibcb.ac.cn (R.Z.),  
mzhang@ust.hk (M.Z.)

### In Brief

Cells often concentrate limited amounts of enzymes at specific subcellular regions for distinct functions. Zhu et al. show that the small GTPase regulatory enzymes GIT and PIX autonomously form phase-separated condensates without the need for scaffolding molecules. GIT/PIX condensates are modular and positioned at specific cellular compartments for distinct signaling.

### Highlights

- Small GTPase regulatory enzymes GIT and PIX bind to each other very tightly
- The GIT/PIX complex forms highly concentrated condensates via phase separation
- Formation of GIT/PIX condensates does not require other scaffold molecules
- GIT/PIX condensates are modular for signaling in distinct cellular compartments



## Article

# GIT/PIX Condensates Are Modular and Ideal for Distinct Compartmentalized Cell Signaling

Jinwei Zhu,<sup>1,2,6,\*</sup> Qingqing Zhou,<sup>3,6</sup> Yitian Xia,<sup>1</sup> Lin Lin,<sup>1,2</sup> Jianchao Li,<sup>3</sup> Mengjuan Peng,<sup>1,4</sup> Rongguang Zhang,<sup>1,4,\*</sup> and Mingjie Zhang<sup>3,5,7,\*</sup>

<sup>1</sup>State Key Laboratory of Molecular Biology, Shanghai Institute of Biochemistry and Cell Biology, Center for Excellence in Molecular Cell Science, Chinese Academy of Sciences, Shanghai 200031, China

<sup>2</sup>Bio-X Institutes, Key Laboratory for the Genetics of Developmental and Neuropsychiatric Disorders, Ministry of Education, Shanghai Jiao Tong University, Shanghai 200240, China

<sup>3</sup>Division of Life Science, State Key Laboratory of Molecular Neuroscience, Hong Kong University of Science and Technology, Clear Water Bay, Kowloon, Hong Kong, China

<sup>4</sup>School of Life Science and Technology, ShanghaiTech University, 100 Haik Road, Shanghai 201210, China

<sup>5</sup>Center of Systems Biology and Human Health, Hong Kong University of Science and Technology, Clear Water Bay, Kowloon, Hong Kong, China

<sup>6</sup>These authors contributed equally

<sup>7</sup>Lead Contact

\*Correspondence: jinwei.zhu@sjtu.edu.cn (J.Z.), rgzhang@sibcb.ac.cn (R.Z.), mzhang@ust.hk (M.Z.)  
<https://doi.org/10.1016/j.molcel.2020.07.004>

## SUMMARY

Enzymes or enzyme complexes can be concentrated in different cellular loci to modulate distinct functional processes in response to specific signals. How cells condense and compartmentalize enzyme complexes for spatiotemporally distinct cellular events is not well understood. Here we discover that specific and tight association of GIT1 and  $\beta$ -Pix, a pair of GTPase regulatory enzymes, leads to phase separation of the complex without additional scaffolding molecules. GIT1/ $\beta$ -Pix condensates are modular in nature and can be positioned at distinct cellular compartments, such as neuronal synapses, focal adhesions, and cell-cell junctions, by upstream adaptors. Guided by the structure of the GIT/PIX complex, we specifically probed the role of phase separation of the enzyme complex in cell migration and synapse formation. Our study suggests that formation of modular enzyme complex condensates via phase separation can dynamically concentrate limited quantities of enzymes to distinct cellular compartments for specific and optimal signaling.

## INTRODUCTION

Signals are often initiated, amplified, and transduced at specific subcellular regions with temporal requirements in living cells. Spatiotemporal cell signaling requires enzymes to be concentrated at defined subcellular compartments so that limited amounts of enzymes can satisfy the required catalytic activity and substrate specificity. A traditional view is that enzymes can be concentrated at specific subcellular regions by binding to their cognate interacting proteins in accordance with the traditional thermodynamic binding equilibrium, although many cellular observations cannot be satisfactorily explained by such a traditional view. Emerging evidence suggests that formation of membrane-less compartments, also known as biomolecular condensates, via liquid-liquid phase separation is another mechanism for cells to concentrate biomolecules, including enzymes, at specific subcellular regions (Banani et al., 2017; Chen et al., 2020; Feng et al., 2019; Hyman et al., 2014; Shin and Brangwynne, 2017). Membrane-less condensates are widespread in cells and include cellular machineries such as P gran-

ules (Brangwynne et al., 2009), nucleoli (Brangwynne et al., 2011), centrosomes (Woodruff et al., 2015, 2017), pre- and post-synaptic signaling apparatuses (Wu et al., 2019; Zeng et al., 2016, 2018, 2019), and stress granules (Molliex et al., 2015; Patel et al., 2015). Membrane-less biomolecular condensates display many unique features with respect to canonical stoichiometric assemblies of molecular complexes as well as membrane-enclosed cellular compartments (Banani et al., 2017; Chen et al., 2020; Feng et al., 2019; Shin and Brangwynne, 2017).

Intuitively, formation of biomolecular condensates can massively enrich reactants and enzymes within the small volume of a subcellular compartment and, therefore, dramatically modify the chemical reactions involved. Although enormous progress has been made, the mechanisms driving formation of biomolecular condensates are far from clear. Based on many decades of research of phase separation of chemical polymers and the recent explosive development of the field of biological condensates, formation of biomolecular condensates requires the presence of multivalent interactions between the molecules in each



system (Banani et al., 2017; Banjade and Rosen, 2014; Chen et al., 2020; Choi et al., 2020; Li et al., 2012). Additionally, it is commonly believed that formation of biomolecular condensates also requires highly abundant organizing molecules, such as scaffold proteins, proteins with a low-complexity sequence, or nucleic acids (Banani et al., 2017; Ditlev et al., 2018). Most biological signaling processes are highly specific and sensitive to changes in protein component or concentration under physiological conditions. Paradoxically, the majority of reported biological condensates involve or are even dominated by low-complexity or intrinsically disordered sequences in a diverse set of proteins (Chong et al., 2018; Jain and Vale, 2017; Wang et al., 2018). The interactions mediated by the low-complexity/intrinsically disordered sequences are often with low specificities. Several recent studies have found that highly specific and strong molecular interactions are also important for formation of various biomolecular condensates, such as synaptic signaling machineries (Wu et al., 2019; Zeng et al., 2016, 2018), cell polarity regulatory complexes (Shan et al., 2018), and autophagosome formation (Fujioka et al., 2020); formation of these molecular assemblies requires highly abundant scaffold proteins.

GIT and PIX are Arf-specific GTPase-activating proteins (GAPs) and Rho-specific guanine nucleotide exchange factors (GEFs), respectively (Manser et al., 1998; Premont et al., 1998; Zhou et al., 2016). GIT proteins, including GIT1 and GIT2, share a conserved domain architecture that consists of an N-terminal zinc-finger ArfGAP domain, an ankyrin repeat (ANK) domain, a Spa2 homology domain (SHD), a coiled-coil domain, and a C-terminal focal adhesion targeting (FAT) domain (Figure 1A). Each PIX protein, including  $\alpha$ -Pix and  $\beta$ -Pix, contains an N-terminal SH3 domain followed by the catalytic Dbl homology (DH) and pleckstrin homology (PH) domain tandem, the GIT-binding domain (GBD), and a C-terminal coiled-coil (CC) domain (Figure 1A). GIT and PIX can self-associate through their respective coiled-coil domains so that the GIT/PIX complex can form very large molecular mass oligomers (Premont et al., 2004; Zhao et al., 2000). GIT and PIX can bind to many partner proteins and regulate diverse cellular processes, such as synaptic development and signaling, focal adhesion formation and dynamics, cell polarity and migration, immune responses, and so on (Zhou et al., 2016), presumably by functioning as regulatory hubs for the Arf and Rho families of GTPases at specific cellular locations. It is perhaps not surprising that mutations of *GIT* or *PIX* can cause different human diseases, including cancer (Peng et al., 2013), psychiatric disorders (Kutsche et al., 2000; Won et al., 2011), and autoimmune diseases (Chang et al., 2014), among others. Therefore, it is of great importance to understand how the GIT/PIX complex might be assembled and how it can modulate diverse cellular processes in different cellular compartments in response to various signals.

In this work, we show that GIT and PIX bind to each other with a very high affinity ( $K_D$ ,  $\sim 20$  nM). We also elucidate the structural basis underlying the strong interaction between GIT and PIX. Unexpectedly, the GIT1/ $\beta$ -Pix complex undergoes phase separation, forming highly concentrated enzyme condensates *in vitro* and in living cells without help from additional scaffolding molecules. GIT1/ $\beta$ -Pix condensates can be recruited to focal adhesions or synapses by binding to Paxillin or Shank3, respectively.

Therefore, GIT/PIX enzymatic complexes can autonomously form modular condensates capable of being targeted to specific subcellular compartments by upstream adaptor proteins. Formation of modular enzymatic condensates provides a mechanism for cells to concentrate limited amounts of enzymes at specific subcellular regions for distinct functions.

## RESULTS

### The GAP-ANK-SHD Tandem of GITs Binds to $\beta$ -Pix with a Very High Affinity

An earlier study reported that the SHD domain of GIT1 binds to a fragment of  $\beta$ -Pix (amino acids [aa] 496–554) (Zhao et al., 2000). We verified this interaction using purified proteins. An isothermal titration calorimetry (ITC)-based assay showed that the SHD domain of GIT1 binds to  $\beta$ -Pix<sup>494–555</sup> with a dissociation constant ( $K_D$ ) of  $\sim 0.15$   $\mu$ M (Figure 1B). A 21-residue fragment of  $\beta$ -Pix (aa 528–548; referred to as GBD) was found to be sufficient for binding to the GIT1 SHD ( $K_D$ ,  $\sim 0.18$   $\mu$ M) (Figures 1B and 1C). Further truncation of the  $\beta$ -Pix GBD at either end impaired its binding to the GIT1 SHD (Figure 1B); thus, the 21-residue GBD is the minimal and complete GIT1 binding region of  $\beta$ -Pix. Unexpectedly, we found that a longer fragment of GIT1 that includes the GAP domain, ANK domain, and SHD (i.e., the GAS tandem) binds to the  $\beta$ -Pix GBD with an  $\sim 10$ -fold higher affinity than the SHD alone ( $K_D$ ,  $\sim 0.015$   $\mu$ M; Figures 1B and 1D), indicating that the GAP domain, ANK domain, and SHD of GIT1 may form a structural supramodule for binding to  $\beta$ -Pix. We further showed that the GIT2 GAS tandem bound to the  $\beta$ -Pix GBD with a similar affinity ( $K_D$ ,  $\sim 0.027$   $\mu$ M; Figure 1B).

### The Structural Basis Governing the Specific GIT/PIX Interactions

To elucidate the molecular basis underlying the specific GIT/PIX interactions, we tried to crystallize the  $\beta$ -Pix GBD in complex with the GAS tandem of GIT1 or GIT2. We were able to obtain crystals of the GAS tandem of GIT2 (but we were unable to do so with GIT1 GAS) in complex with a synthetic  $\beta$ -Pix GBD peptide, but the complex crystals only diffracted to  $\sim 4$ - to  $5$ - $\text{\AA}$  resolution. After numerous trials, we discovered that the GIT2 GAS/ $\beta$ -Pix GBD complex prepared from a GIT2 GAS mutant bearing two point mutations in a predicted loop region (S255A/S256A, denoted GAS<sup>S255A/S256A</sup>; the complex is referred to as the GIT2-GAS/ $\beta$ -Pix GBD complex hereafter for simplicity) could crystallize, and crystals were diffracted to  $2.8$ - $\text{\AA}$  resolution. The complex structure was solved by the molecular replacement method using the structure of the GAP-ANK tandem of ACAP1 (PDB: 3JUE) as the search model (Table S1).

The structure of the GIT2-GAS/ $\beta$ -Pix GBD complex explains how the GAP domain, ANK domain, and SHD of GIT1 form a supramodule with enhanced binding to the  $\beta$ -Pix GBD. The structure of the GIT2 GAP domain in the complex is very similar to that of the ASAP3 GAP domain observed in an Arf6/ASAP3 complex (Ismail et al., 2010; Figures S1A and S1B). Superimposition of the structure of GAP<sup>GIT2</sup> with that of GAP<sup>ASAP3</sup> shows that a conserved arginine of GAP<sup>GIT2</sup>, R39<sup>GIT2</sup>, aligns well with the arginine finger of ASAP3, R469<sup>ASAP3</sup>, which is required for GTP hydrolysis (Figure S1B). This structural analysis is

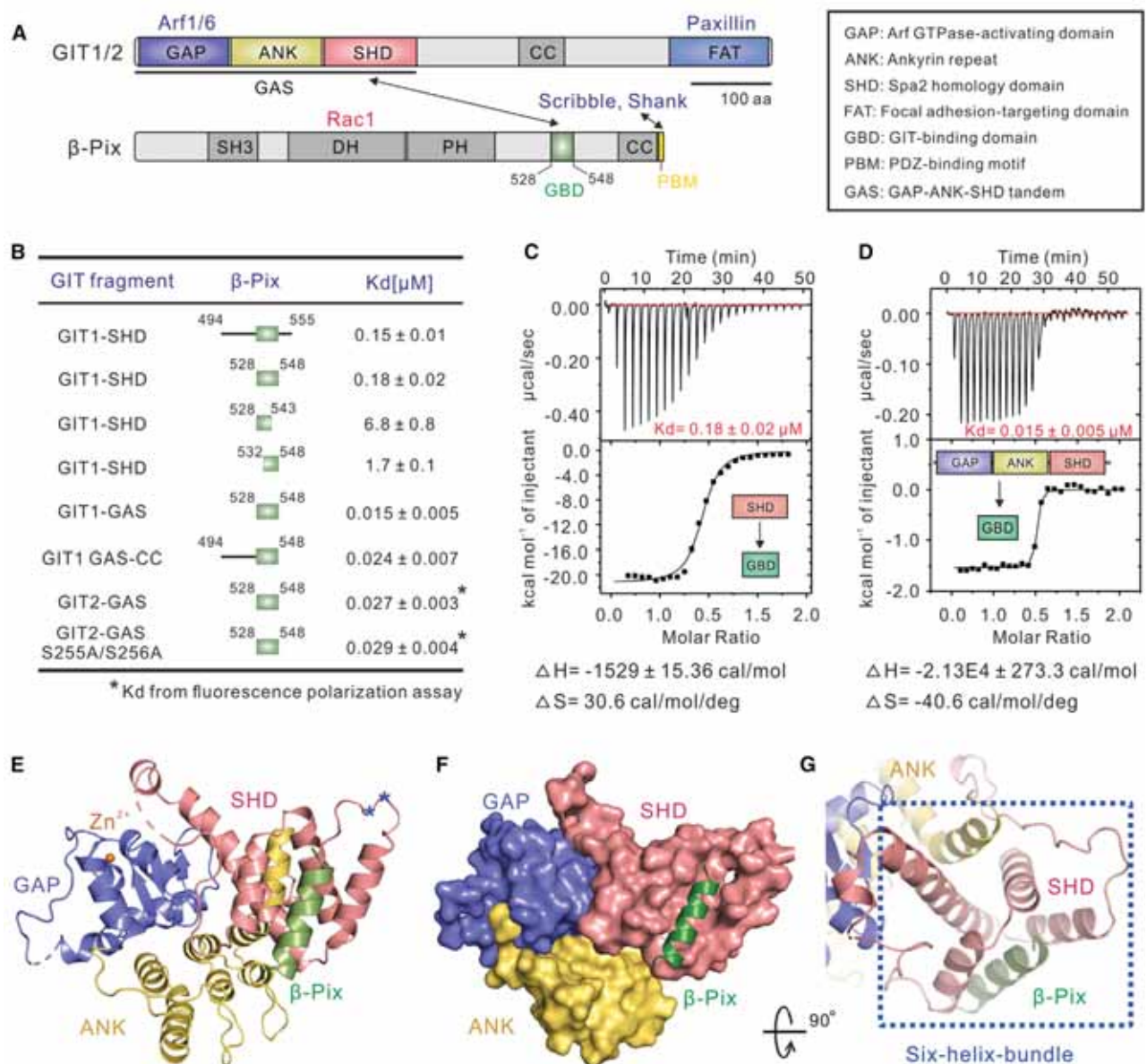


**Figure 1. Biochemical and Structural Characterization of GIT/PIX Interaction**

(A) Schematic diagram showing the domain organization of the GIT1,2 and β-Pix proteins. The GIT/PIX interaction is indicated by a two-way arrow. The color-coding scheme is used throughout the paper. The domain keys are also shown.

(B) The dissociation constants of the interactions between various forms of GIT and β-Pix, obtained from ITC-based assays. Binding of the WT and mutant form of GIT2 GAP-ANK-SHD (GAS) to β-Pix 528–548 (GBD) was measured using a fluorescence polarization assay because of very little heat release of the reaction.

(C and D) ITC curves showing binding of β-Pix GBD to the isolated SHD domain (C) and the GAS tandem (D) of GIT1.

(E) Ribbon diagram representation of the GIT2 GAS/β-Pix GBD complex structure. Residues S255 and S256, substituted with Ala during crystal preparation, are indicated by blue asterisks.

(F) Combined surface and ribbon representation of the GIT2 GAS/β-Pix GBD complex structure showing that the GAP domain, ANK domain, and SHD couple tightly to each other, forming a supramodule.

(G) A six-helix bundle formed by αC<sup>ANK</sup> of ANK, the four helices from the SHD, and the β-Pix GBD helix.

See also Figure S1 and Table S1.

consistent with previous findings showing that GIT proteins possess GAP activities toward Arf1 and Arf6 (Premont et al., 1998; Vitale et al., 2000) and that R39 is critical for GAP activity

(Hoefen and Berk, 2006; Mandiyani et al., 1999). The ANK domain contains three ANKs and a C-terminal α helix (αC<sup>ANK</sup>) that takes an ~90° bend toward α3B of ANK (Figure S1C). The concave

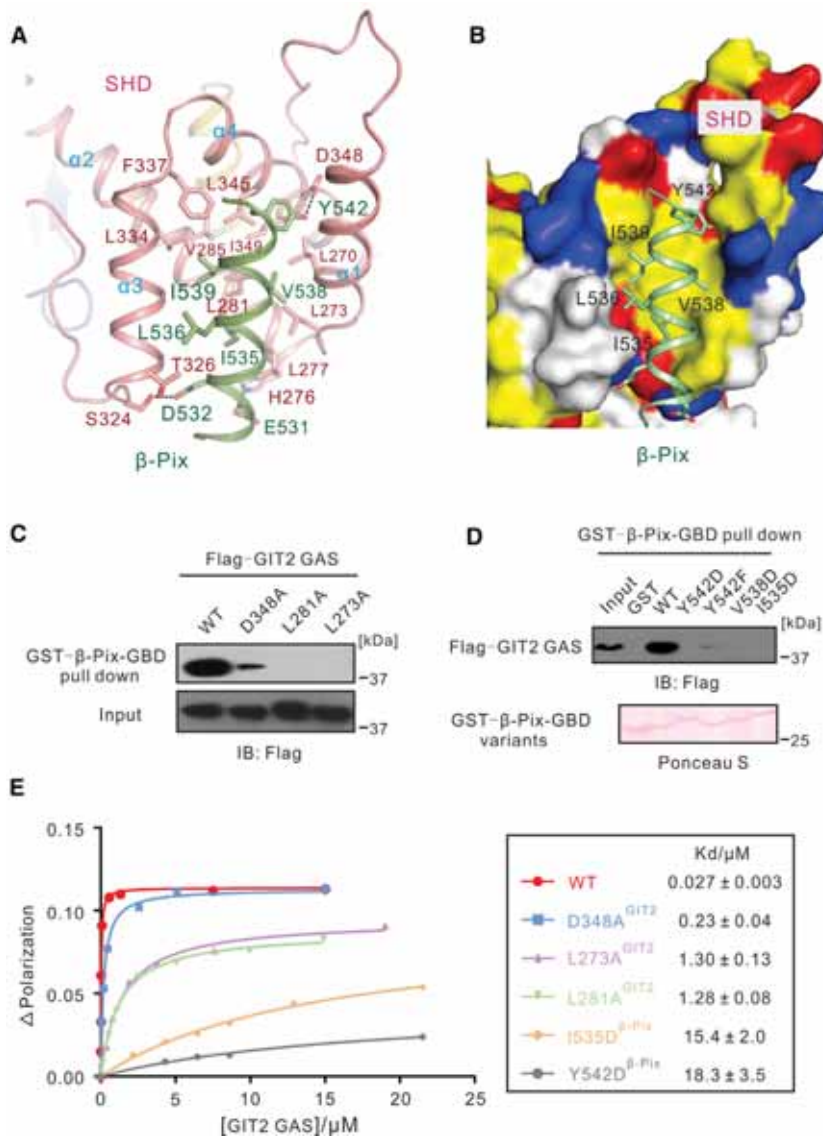


**Figure 2. Structural Details of the GIT2/β-Pix Interface**

(A) Detailed interactions between GIT2 GAS and the β-Pix GBD.

(B) Combined surface and ribbon representation of the GIT2/β-Pix interface, showing that binding is mainly mediated by hydrophobic interactions and supplemented by hydrogen bonds. In the surface diagram, hydrophobic residues are shown in yellow, positively charged residues in blue, negatively charged residues in red, and the rest in gray.

(C) GST-pull down assays showing that key residues of GIT2 GAS involved in the GIT2 GAS and β-Pix GBD interface are required for the interaction.

(D) GST-pull down assays showing that key residues of β-Pix GBD required for the GIT2/β-Pix interaction.

(E) Fluorescence polarization-based measurement of binding affinities of WT and mutant GIT2 GAS to WT and mutant β-Pix GBD peptides.

See also [Figures S1](#) and [S2](#).

indicating that formation of the GITs GAS supramodule may stabilize the conformation of the SHD and, thus, enhance the interactions between GITs and β-Pix.

The GIT2/β-Pix interaction is mainly mediated by hydrophobic interactions. I535, L536, V538, I539, and Y542 from the β-Pix GBD form hydrophobic contacts with L270, L273, L277, L281, V285, L334, F337, L345, and I349 from the GIT2 SHD ([Figures 2A](#) and [2B](#)). Additional polar interactions (e.g., the hydrogen bond formed between Y542<sup>β-Pix</sup> and D348<sup>GIT2</sup>; [Figure 2A](#)) further support the binding specificity of the complex. Importantly, the residues involved in the binding interface are highly conserved in GITs and PIX ([Figures S2A](#) and [S2B](#)), implying indispensable roles of the GIT/PIX interactions in the animal kingdom. A series of mutations on GIT2 GAS and the β-Pix GBD were generated to

groove of ANK is unoccupied and available for potential target binding ([Figures 1E](#) and [S1C](#)). The SHD in the complex is formed by four consecutive  $\alpha$  helices ( $\alpha 1$ – $\alpha 4$ ) ([Figure S1D](#)).

In line with our biochemical data, the GAP domain, ANK domain, and SHD of GIT2 interact with each other intimately to form a structural supramodule ([Figures 1E](#) and [1F](#)). S255 and S256 are located at the loop between ANK and the SHD and are away from the GIT2/β-Pix interface (indicated by asterisks in [Figure 1E](#)), so the mutations used to facilitate crystallization should not affect the structure of the GAS tandem and its binding to β-Pix. Our biochemical data confirmed that GIT2-GAS<sup>S255A/S256A</sup> bound to the β-Pix GBD with a similar affinity compared with that of wild-type (WT) GIT2-GAS ([Figure 1B](#)). In the complex, the β-Pix GBD forms an  $\alpha$ -helix and interacts with the GIT2 SHD. A stable six-helix bundle is formed by the β-Pix GBD  $\alpha$  helix, four helices of the GIT2 SHD, and  $\alpha$ C<sup>ANK</sup> ([Figure 1G](#)),

verify the roles of these residues in complex formation. To minimize possible perturbation of the overall folding of GIT2-GAS, we substituted L273<sup>GIT2</sup> in  $\alpha 1$  or L281<sup>GIT2</sup> in  $\alpha 2$  with Ala. Both mutations impaired GIT2 binding to the β-Pix GBD ([Figures 2C](#) and [2E](#)). Reciprocally, neither the I535D nor the V538D mutant of the β-Pix GBD was capable of binding to GIT2 GAS (more dramatic amino acid substitutions were chosen because the β-Pix GBD is a short peptide fragment; [Figures 2D](#) and [2E](#)). Substitution of Y542<sup>β-Pix</sup> with Asp also impaired its binding to GIT2 GAS ([Figures 2D](#) and [2E](#)).

#### GIT1 Undergoes Phase Separation *In Vitro* and in Cells

Interestingly, we observed that the full-length WT GIT1 solution turned turbid above certain concentrations at room temperature. The turbid solution became clear again upon cooling the protein sample on ice. We sparsely labeled purified GIT1 with the Cy3

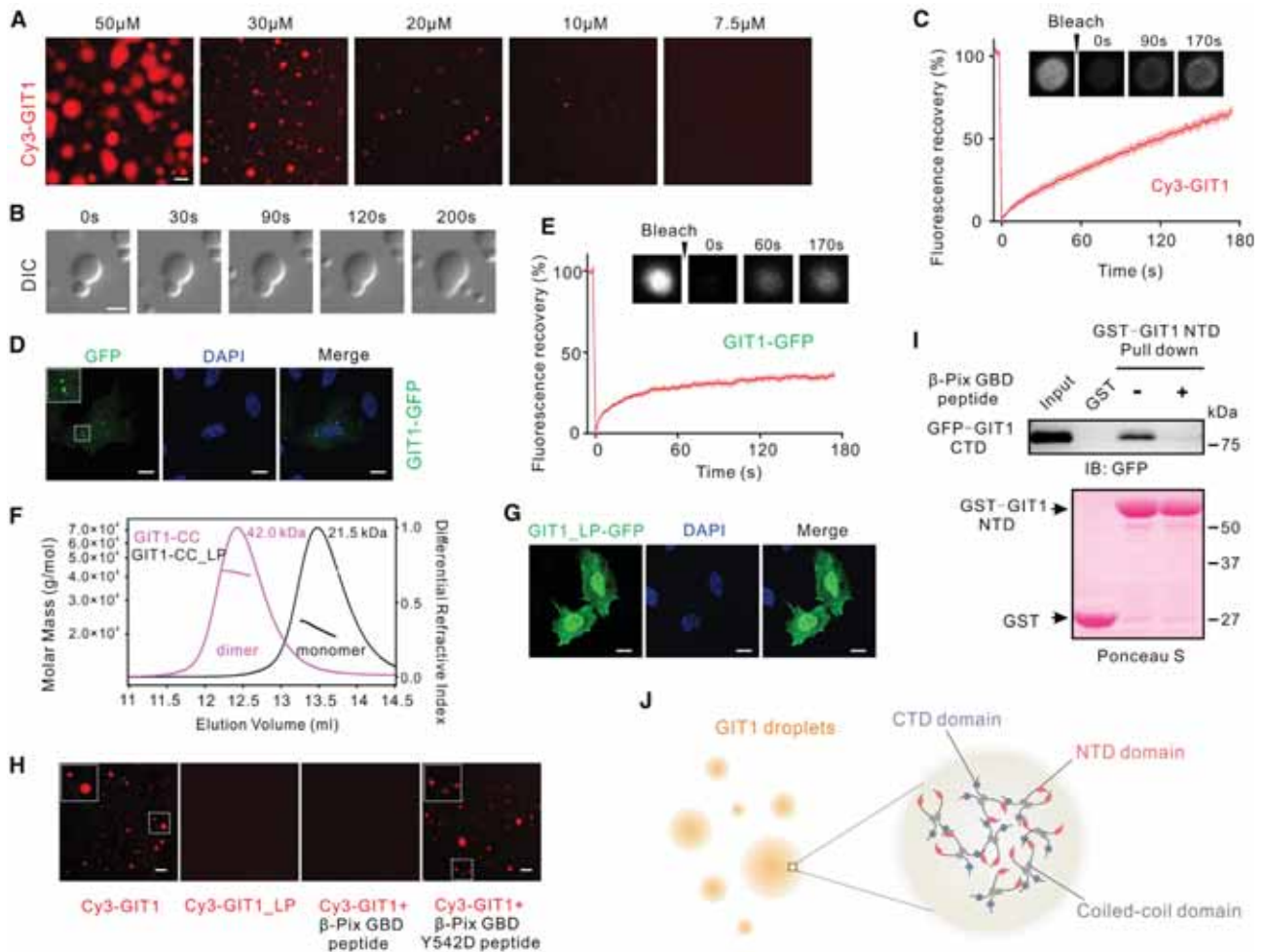


**Figure 3. GIT1 Undergoes Phase Separation *In Vitro* and in Living Cells**

(A) Fluorescence images showing that the full-length GIT1 protein underwent phase separation at the indicated concentrations. GIT1 was sparsely labeled by Cy3 at 1%.  
 (B) DIC images showing that GIT1 condensed droplets fused with each other, forming larger droplets over time.  
 (C) FRAP analysis showing that GIT1 in condensed droplets dynamically exchanged with those in the dilute phase.  
 (D) Representative images showing that expression of GIT1-GFP in HeLa cells produced many bright and spherical puncta.  
 (E) FRAP analysis showing that GIT1-GFP in the spherical puncta dynamically exchanged with those in the cytoplasm.  
 (F) Fast protein liquid chromatography (FPLC)-coupled static light-scattering analysis showing that WT GIT1-CC formed a stable dimer in solution, whereas the LP mutant of GIT1-CC is a monomer.  
 (G) Representative images showing that expression of the GFP-GIT1<sub>LP</sub> mutant in HeLa cells did not form any puncta.  
 (H) Fluorescence images showing that the GIT1<sub>LP</sub> mutant cannot form phase separation at a concentration of 20 μM. Binding of the β-Pix GBD peptide, but not the β-Pix GBD<sub>Y542D</sub> peptide, abolished phase separation of GIT1.  
 (I) Glutathione S-transferase (GST) pull-down assay showing that the N-terminal fragment (aa 1–371, NTD) of GIT1 binds to the C-terminal fragment of GIT1 (aa 371–end, CTD). Addition of the β-Pix GBD peptide impaired the interaction between NTD and CTD of GIT1.  
 (J) A model depicting the mechanism of GIT1 phase separation.  
 Scale bars, 5 μm. See also [Figures S3 and S4](#).

fluorophore and investigated the turbid solution under a confocal microscope. Cy3-GIT1 formed phase-separated droplets with spherical shapes in a concentration-dependent manner ([Figure 3A](#)). Differential interference contrast (DIC) microscopy images further showed that small droplets could fuse into larger ones over time ([Figure 3B](#)). Fluorescence recovery after photobleaching (FRAP) analysis of Cy3-GIT1 droplets showed that

GIT1 molecules can exchange freely between the condensed and dilute phases ([Figure 3C](#)). Next we tested whether GIT1 can undergo phase separation in living cells. When GIT1-GFP (i.e., GFP fused to the C-terminal end of GIT1) was overexpressed in HeLa cells, spherical GIT1-GFP puncta were observed ([Figure 3D](#)). A FRAP assay showed that GIT1-GFP within these puncta can exchange with the surrounding dilute

cytoplasmic population (Figure 3E), indicating that GIT1-GFP formed membrane-less condensates in cells.

We next dissected the molecular mechanism that governs GIT1 phase separation. In many biological systems, proteins containing intrinsic disordered regions (IDRs) can phase separate under physiological conditions (Banani et al., 2017; Shin and Brangwynne, 2017; Wright and Dyson, 2015). GIT1, however, does not contain long IDR stretches that have propensities to undergo phase separation (Figures S2C and S2D). Therefore, it is unlikely that GIT1 phase separation is driven by IDRs. Because the coiled-coil domain of GIT1 mediates its dimerization (Schlenker and Rittinger, 2009; Figure 3F), we first investigated whether this interaction is required for GIT1 phase separation. A triple mutant of GIT1 (L438P, L459P, L466P; referred to as the LP mutant hereafter) converted the dimeric GIT1-CC into a monomer (Figure 3F). The GIT1\_LP mutant completely lost its capacity to form condensed droplets *in vitro* and in HeLa cells (Figures 3G, 3H, and S3), indicating that GIT1 dimer formation is essential for its phase separation. However, dimerization alone is likely not sufficient to support GIT1 phase separation because multivalent inter-molecular interactions are known to be required for phase separation of biomolecular complexes (Banani et al., 2017; Li et al., 2012). Therefore, we searched for additional molecular interaction(s) with GIT1. We found that the N-terminal region (NTD) of GIT1 (aa 1–371, GIT1-NTD corresponding to the GAS tandem) specifically binds to its C-terminal half (aa 371–end, GIT1-CTD) (Figure 3I). Because the coiled-coil domain of GIT1 adopts a parallel conformation during its dimerization, the binding between NTD and CTD of GIT1 is likely inter-molecular in nature, based on the topology of the protein conformation. Interestingly, addition of the  $\beta$ -Pix GBD peptide blocked the interaction between NTD and CTD of GIT1 (Figure 3I), likely because the  $\beta$ -Pix binding site and the CTD binding site on GIT1 NTD overlap. It is predicted that the  $\beta$ -Pix GBD peptide should be able to prevent GIT1 phase separation by blocking GIT1 oligomerization. Indeed, addition of the  $\beta$ -Pix GBD peptide abolished the phase separation of Cy3-GIT1 *in vitro*, whereas a mutant  $\beta$ -Pix GBD peptide (GBD\_Y542D), which is deficient in GIT1-binding, had no effect on GIT1 phase separation (Figure 3G). We conclude that coiled coil-mediated dimerization and the interaction between GIT1 NTD and CTD contribute to the phase separation of GIT1 (Figure 3J). Notably, the longest isoforms of GIT2 and GIT1 share highly conserved domain organizations and sequence identities, but that GIT1 contains an additional octamer insertion sequence in its GAS tandem (Figure S4). We generated a GIT2-mimicking mutant of GIT1 that lacks the octamer insertion (GIT1\_del8) and found that GIT1\_del8, alone or in complex with PIX, displayed similar phase separation as WT GIT1 (Figure S4). Thus, GIT2, like GIT1, may also phase separate alone or in complex with PIX.

### Binding of $\beta$ -Pix to GIT1 Promotes Phase Separation of GIT1

Because  $\beta$ -Pix is a strong binding partner of GIT1 and can form stable trimer via its coiled-coil domain (Schlenker and Rittinger, 2009), formation of the GIT1/ $\beta$ -Pix complex might further increase GIT1 oligomerization and, in turn, promote phase separation of GIT1. Indeed, mixing equal molar amounts of Cy3-labeled

GIT1 with Alexa 488-labeled  $\beta$ -Pix led to formation of condensed liquid droplets enriched with both proteins (Figure 4A). Importantly, addition of  $\beta$ -Pix lowered the threshold concentration for GIT1 to undergo phase separation and dramatically increased the number of condensed droplets of GIT1 (Figure 3A versus Figure 4A).  $\beta$ -Pix alone, at a concentration up to 100  $\mu$ M, did not undergo phase separation (Figure S3I). When GIT1-GFP and RFP- $\beta$ -Pix were co-expressed in HeLa cells, we observed many bright and completely overlapping spherical puncta enriched with both proteins (Figure 4B; quantified in Figure S3). No puncta were observed in cells expressing RFP- $\beta$ -Pix alone (Figures 4B and S3), indicating that  $\beta$ -Pix by itself could not form a condensed phase. FRAP analysis showed that the GIT1-GFP signal within the puncta could be recovered after photobleaching, but only to approximately 20% of its original intensity within a few minutes (Figure 4C). Notably, the exchange rate of GIT1 between the condensed phase and the dilute cytoplasmic phase was considerably slower than that reported in other phase separation systems in cells (Sabari et al., 2018; Woodruff et al., 2017; Zeng et al., 2016), suggesting that the GIT1/ $\beta$ -Pix condensates are less dynamic, possibly because of the very tight binding between the two proteins. The  $\beta$ -Pix\_Y542D mutant has an  $\sim$ 5,000-fold reduction in binding to GIT1 (Figure S3J). Interestingly, when GIT1-GFP was co-expressed with  $\beta$ -Pix\_Y542D, the recovery speed of GIT1-GFP signal after photobleaching was much faster than that of GIT1 co-expressed with WT  $\beta$ -Pix (Figures 4C and S3K). Y542 of  $\beta$ -Pix has been reported to be phosphorylated in cells by focal adhesion kinase or Src (Feng et al., 2006; Mayhew et al., 2007). It is tempting to speculate that phosphorylation of  $\beta$ -Pix at Y542 may be a regulatory switch for GIT1/ $\beta$ -Pix condensates to disperse, a hypothesis that needs to be tested in the future.

We next investigated the role of  $\beta$ -Pix valency in promoting phase separation of the GIT1/ $\beta$ -Pix complex. The coiled-coil domain of  $\beta$ -Pix is a trimer in solution (Schlenker and Rittinger, 2009). Guided by the structure of  $\beta$ -Pix-CC (PDB: 2W6B), we designed a two-point mutant of  $\beta$ -Pix-CC (i.e., V601D, V629D; referred to as the VD mutant hereafter) capable of converting trimeric  $\beta$ -Pix-CC into a monomer (Figures 4D and 4E). Mixing Alexa 488-labeled monomeric  $\beta$ -Pix\_VD with Cy3-GIT1 did not promote phase separation of GIT1; instead, it eliminated phase separation of GIT1 (Figure 4F). Additionally, when GIT1-GFP and RFP- $\beta$ -Pix\_VD were co-expressed in cells, no phase-separated puncta could be observed (Figure S3). It is likely that the monomeric  $\beta$ -Pix\_VD, analogous to the  $\beta$ -Pix GBD peptide (Figures 3H and 3I), can specifically bind to GIT1 and, consequently, disrupt the NTD and CTD binding-mediated oligomerization of GIT1. The above data indicate that phase separation of the GIT1/ $\beta$ -Pix complex is driven by formation of large molecular network contributed by coiled-coil domain-mediated multimerization of GIT1 and  $\beta$ -Pix as well as the very strong interaction between GIT1 and  $\beta$ -Pix (Figure 4G). Because GIT1 alone and GIT1/ $\beta$ -Pix are able to form condensates, we constructed a phase diagram of GIT1/ $\beta$ -Pix condensates by fixing the concentration of GIT1 or  $\beta$ -Pix and gradually increasing the other protein to show that there are no two separated types of condensates co-existed in the mixtures (Figure S5).

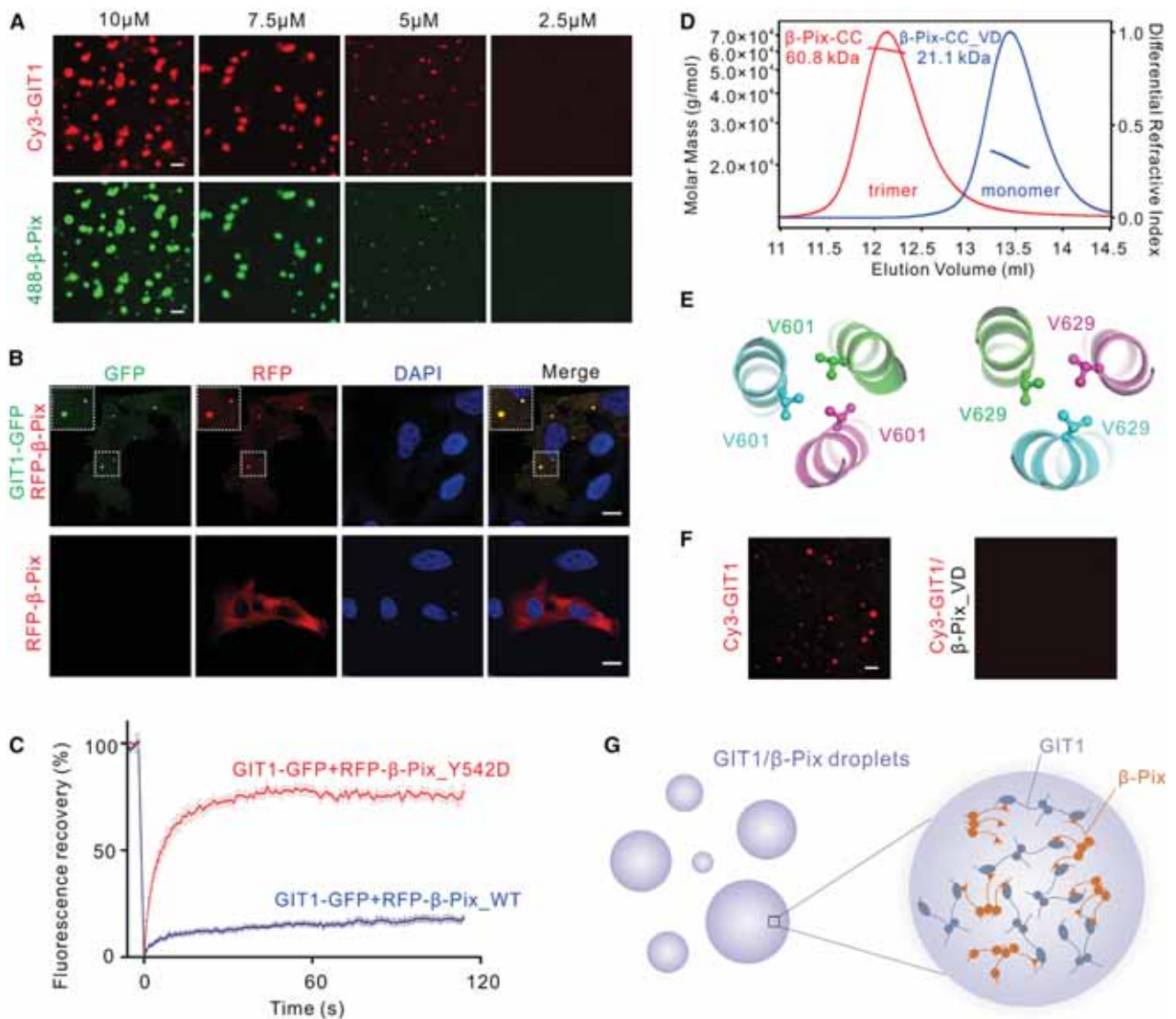


**Figure 4. Formation of GIT1/β-Pix Condensates**

(A) Fluorescence images showing that a mixture of GIT1 and β-Pix (both proteins are in their full-length forms) led to phase separation at the indicated concentrations. GIT1 and β-Pix were labeled with Cy3 and Alexa 488 at 1%, respectively. Scale bar, 5 μm.

(B) Representative images showing that co-expression of GIT1-GFP and RFP-β-Pix in HeLa cells produced multiple spherical puncta, whereas RFP-β-Pix alone was diffused in the cytoplasm. Scale bar, 5 μm.

(C) FRAP analysis showing that GIT1-GFP in the puncta, when co-expressed with WT RFP-β-Pix, exchanged slowly with the protein in dilute cytoplasm. Signal recovery was also very limited. In contrast, exchange of GIT1-GFP between the puncta and cytoplasm, when co-expressed with the Y542D mutant of β-Pix, was much faster, and signal recovery was also much higher.

(D) FPLC-coupled static light-scattering analysis showing that WT β-Pix-CC forms a stable trimer in solution and that the VD mutant is a monomer.

(E) Close-up view of the interactions between V601 and V629 in the β-Pix trimer (PDB: 2W6B).

(F) Fluorescence images showing that the β-Pix\_VD mutant abolished phase separation of GIT1. The assay was performed under the same condition as in Figure 3A, with each protein at a concentration of 20 μM.

(G) A schematic showing the interaction network formed by GIT1 and β-Pix in the condensates. Scale bar, 5 μm.

See also Figures S3–S5.

### Paxillin's Connection with the GIT1/β-Pix Complex

One of the best-studied roles of the GIT/PIX complexes is that in focal adhesions and cell migration. GIT1 is recruited to focal adhesions via direct binding to Paxillin (Premont et al., 2000; Turner et al., 1999). Paxillin is a multi-domain scaffold protein

composed of five leucine-rich sequences known as LD motifs and four LIM (Lin11, Isl-1, and Mec-3) domains (Figure 5A). The FAT domain of GIT1 has been reported to bind to LD2 and LD4 of Paxillin (Schmalzigaug et al., 2007; Zhang et al., 2008). We confirmed that GIT1 FAT binds to LD2 and LD4 motifs with a

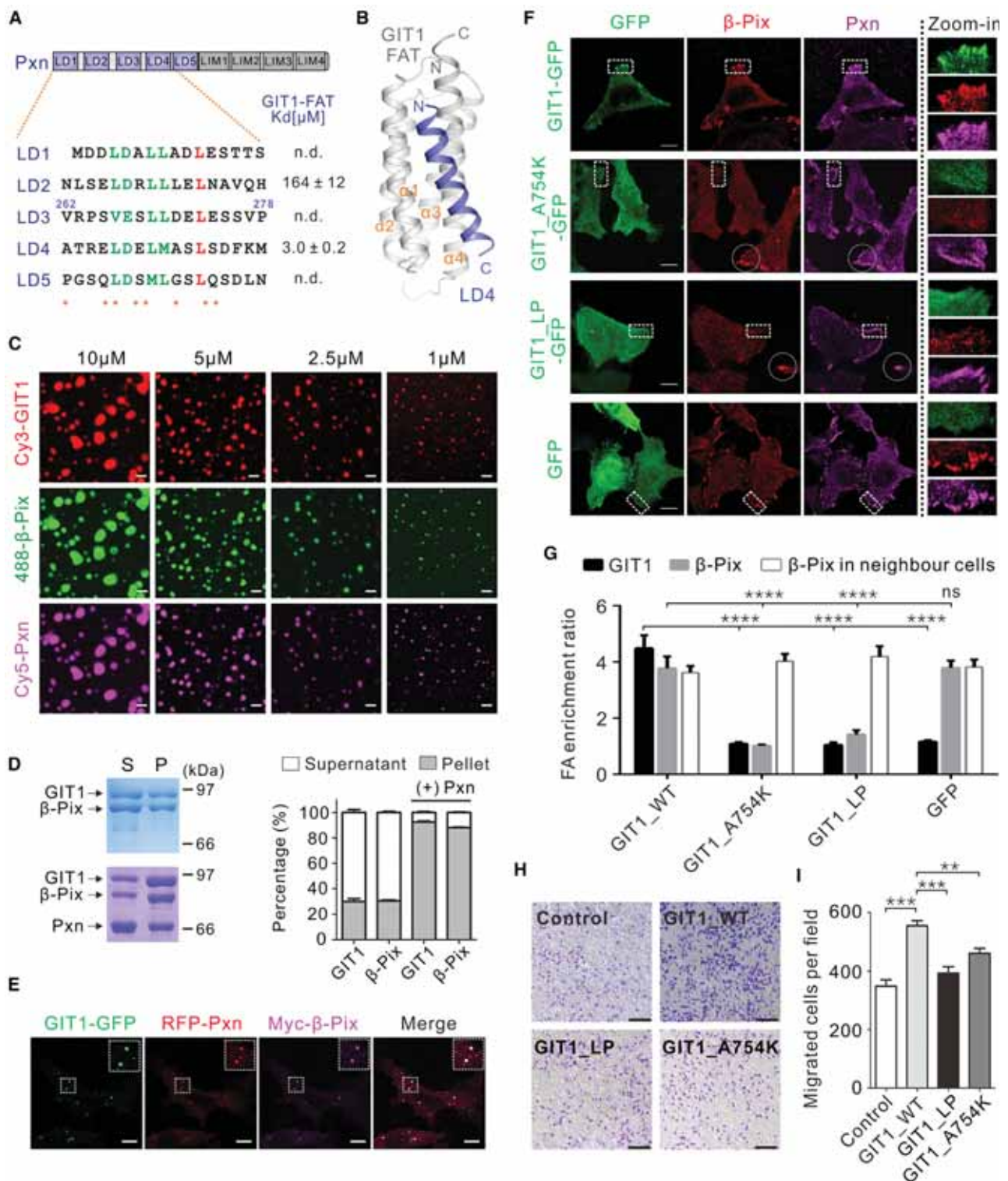


**Figure 5. Paxillin Promotes GIT1/β-Pix Phase Separation**

(A) Schematic diagram showing the domain organization of Paxillin. Sequence alignment of the LD motifs of Paxillin is included. Identical and conserved residues are colored red and green, respectively. Residues involved in the GIT1/Paxillin interaction are indicated by orange dots. The dissociation constants of the interactions between various Paxillin LD motifs and GIT1 FAT, obtained from ITC-based assays, are shown.

(legend continued on next page)

$K_D$  of  $\sim 164 \mu\text{M}$  and  $\sim 3.0 \mu\text{M}$ , respectively. The remaining three Paxillin LD motifs had no detectable binding to GIT1 FAT (Figures 5A and S6A–S6E).

We determined the crystal structure of GIT1 FAT in complex with Paxillin LD4 (Table S1). In the complex, GIT1 FAT adopts a stable four-helix bundle structure that is similar to the apo-FAT structure (Figures 5B and S6F). The LD4 motif forms an  $\alpha$  helix occupying the binding site formed by  $\alpha 1$  and  $\alpha 4$  of GIT1 FAT (Figure 5B). The GIT1 FAT/Paxillin LD4 interface is mainly mediated by hydrophobic interactions (see Figures S6G and S6H for detailed interactions). The GIT1 FAT/Paxillin LD4 interface is similar to those in other FAT/LD interactions, such as the Pyk2/Paxillin, FAK/Paxillin, and CCM3/Paxillin complexes (Figures S6I–S6K). Determination of the GIT1 FAT/Paxillin LD4 complex allowed us to design specific point mutations on GIT1 or Paxillin, leading to complete disruption of complex formation (e.g., L669K<sup>GIT1</sup>, A754K<sup>GIT1</sup>, and F276D<sup>Paxillin</sup>; Figure S6L). These mutations were used to investigate the role of Paxillin in targeting GIT1/ $\beta$ -Pix condensates to focal adhesions and the role of the GIT1/ $\beta$ -Pix condensates in regulating cell migration (see below).

### Paxillin Promotes Phase Separation of the GIT1/ $\beta$ -Pix Complex

Because the LD2 and LD4 motifs bind to GIT1, binding of Paxillin can further expand the valency of the GIT/PIX complex and promote its phase separation. Indeed, addition of full-length Paxillin to the GIT1/ $\beta$ -Pix complex further lowered the threshold concentration for the GIT1/ $\beta$ -Pix complex to undergo phase separation, and Paxillin was also recruited to the condensed phase of the GIT1/ $\beta$ -Pix complex (Figure 5C). Formation of condensed droplets was readily observed at an individual protein concentration of  $1 \mu\text{M}$  or lower (Figure 5C), suggesting that Paxillin/GIT1/ $\beta$ -Pix condensates can form at their physiological concentrations. Consistent with the imaging-based analysis, the amount of GIT1 and  $\beta$ -Pix proteins in the condensed phase (the “pellet” fraction) significantly increased when Paxillin was added in a sedimentation-based assay (Zeng et al., 2016) (from  $\sim 30\%$  to  $\sim 90\%$ ; Figure 5D). To examine whether such co-puncta of three proteins may occur in living cells, GIT1-GFP, RFP-Paxillin, and Myc- $\beta$ -Pix were co-expressed in HeLa

cells. Under a fluorescence microscope, these three proteins formed many co-localized, micrometer-sized spherical puncta in cells (Figure 5E). Notably, GIT1-mediated condensates float in the cytoplasm instead of being associated with focal adhesions, based on the z stack image analysis (Figure S7). Taken together, the above studies demonstrate that the interaction between GIT1 and Paxillin promotes phase separation of the GIT1/ $\beta$ -Pix complex.

### GIT1/ $\beta$ -Pix Condensates Are Recruited to Focal Adhesions and Required for Cell Migration

In cells overexpressing GFP-tagged WT GIT1, endogenous  $\beta$ -Pix was found to be colocalized with GIT1-GFP in Paxillin-marked puncta at focal adhesions (Figure 5F, top row; quantified in Figure 5G). In sharp contrast, overexpression of a Paxillin binding-deficient mutant of GIT1, GIT1<sup>A754K</sup>-GFP, led to dramatically decreased focal adhesion localization of endogenous  $\beta$ -Pix (Figures 5F and 5G, second row). As internal controls, endogenous  $\beta$ -Pix, most likely recruited by endogenous GIT1, could be effectively targeted to focal adhesions in neighboring cells without expression of GIT1<sup>A754K</sup> (Figure 5F, indicated by circles; quantified in Figure 5G) or in cells expressed with GFP alone (Figure 5F, bottom row; quantified in Figure 5G). The reduction of focal adhesion localization of  $\beta$ -Pix in GIT1<sup>A754K</sup>-GFP-expressing cells is likely due to the dominant-negative effect of mutant GIT1 because the mutant can bind to  $\beta$ -Pix with a nanomolar dissociation constant. The above results indicate that GIT1/ $\beta$ -Pix condensates formed by endogenous levels of both enzymes can be targeted to focal adhesions by GIT1-mediated binding to Paxillin.

A critical question is whether formation of clustered GIT1/ $\beta$ -Pix puncta at focal adhesions requires phase separation of GIT1/ $\beta$ -Pix. To address this question, we took advantage of the monomeric GIT1<sub>LP</sub> mutant characterized in Figures 3F–3H. The GIT1<sub>LP</sub> mutant is incapable of undergoing phase separation (Figures 3G and 3H), but the mutant does not affect its binding to  $\beta$ -Pix or Paxillin (Figures 1 and 5A). Thus, the GIT1<sub>LP</sub> mutant can be used to specifically assess the role of GIT1/ $\beta$ -Pix phase separation in targeting of the complex to focal adhesions. Endogenous  $\beta$ -Pix could not be effectively recruited to focal

(B) Ribbon diagram representation of the GIT1 FAT/Paxillin LD4 complex structure.

(C) Fluorescence images showing that mixing Paxillin, GIT1, and  $\beta$ -Pix at the indicated concentrations resulted in condensed droplets with three proteins enriched simultaneously in the condensed phase. Paxillin, GIT1, and  $\beta$ -Pix were labeled with Cy5, Cy3, and Alexa 488, respectively, each at 1%. Scale bars,  $5 \mu\text{m}$ .

(D) Representative SDS-PAGE analysis and quantification data showing the distributions of GIT1 and  $\beta$ -Pix in the supernatant (S) and pellet (P) with or without Paxillin in sedimentation-based assays. The final concentration of each protein was  $5 \mu\text{M}$ . Results are expressed as mean  $\pm$  SD from three independent batches of sedimentation experiments.

(E) Representative images showing co-expression of GFP-GIT1, RFP-Paxillin, and Myc- $\beta$ -Pix in HeLa cells produced many spherical puncta with all three proteins co-localized. Scale bars,  $5 \mu\text{m}$ .

(F) GFP-GIT1 could recruit endogenous  $\beta$ -Pix to focal adhesions marked by an anti-Paxillin antibody in HeLa cells. The GFP-GIT1<sup>A754K</sup> or GFP-GIT1<sub>LP</sub> mutants impaired FA localization of  $\beta$ -Pix. The neighboring non-transfected cells worked as internal controls. GFP only served as the vector control of the experiment. Scale bars,  $5 \mu\text{m}$ .

(G) Quantification of FA enrichment of GFP-GIT1 and its mutants as well as  $\beta$ -Pix, derived from experiment described in (F). For each group, 15 cells from three independent batches were imaged for quantification. The FA enrichment ratio is defined as  $[\text{GFP}_{\text{FA}} \text{ intensity}]/[\text{GFP}_{\text{cytoplasm}} \text{ intensity}]$  or  $[\beta\text{-Pix}_{\text{FA}} \text{ intensity}]/[\beta\text{-Pix}_{\text{cytoplasm}} \text{ intensity}]$  and is expressed as mean  $\pm$  SEM for each group. ns, not significant; \*\*\*\*p < 0.0001, using one-way ANOVA with Dunnett's multiple comparisons test.

(H) Transwell migration assays were performed to measure the cell migration activities of HeLa cells transfected with GFP-GIT1, GFP-GIT1<sup>A754K</sup>, GFP-GIT1<sub>LP</sub>, and the GFP control.

(I) Quantification of cell migration activities of GFP-GIT1 and its mutants from the experiment described in (H). Data are expressed as mean  $\pm$  SEM for each group from six independent experiments. \*\*\*p < 0.001, \*\*p < 0.01, using one-way ANOVA with Dunnett's multiple comparisons test.

See also Figures S6 and S7.

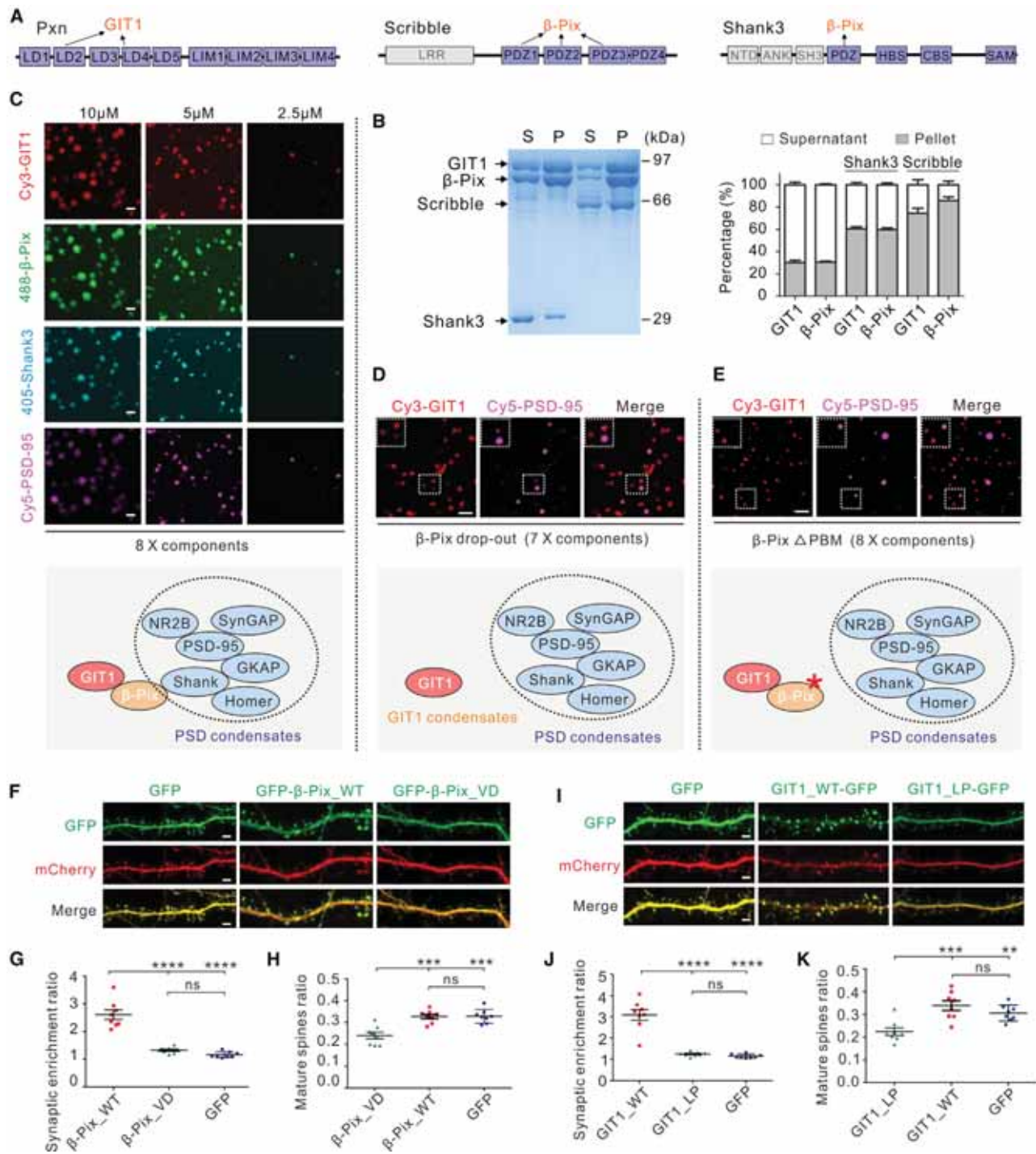


**Figure 6. The GIT1/β-Pix Condensate Module Can Be Recruited to Synapses and Is Required for Dendritic Spine Development**

(A) Schematic diagrams showing the domain organization of Paxillin, Scribble, and Shank3. Domains that interact with GIT1 or β-Pix are indicated. "HBS" and "CBS" in Shank3 stand for Homer binding sequence and cortactin binding sequence, respectively

(B) Sedimentation-based assays showing that Scribble and Shank3 could be enriched and, in return, promote phase separation of GIT1 and β-Pix. Results are expressed as mean ± SD from three independent batches of sedimentation experiments.

(C) Fluorescence images showing that mixing GIT1, β-Pix, and 6x PSD components (PSD-95, GKAP, Shank3, SynGAP, NR2B, and Homer; see the scheme below the images) at the indicated concentrations resulted in condensed droplets with eight proteins enriched simultaneously in the condensed phase. PSD-95, Shank3, GIT1, and β-Pix were labeled with Cy5, iFluor405, Cy3, and Alexa 488, respectively, each at 1%. Scale bars, 5 μm.

(legend continued on next page)

adhesions when cells were expressing the GIT1\_LP-GFP mutant (Figures 5F and 5G, third row).

Because the dynamics of focal adhesions are crucial for cell motility, one would expect that perturbation of recruitment of GIT1/ $\beta$ -Pix condensates to focal adhesions would impair cell migration. Indeed, using a transwell migration assay, we found that expression of GIT1 WT significantly promoted cell migration. In contrast, expression of the GIT1<sup>A754K</sup> or the GIT1\_LP mutant did not promote cell migration (Figures 5H and 5I). The above data suggest that formation of GIT1/ $\beta$ -Pix condensates and Paxillin-mediated targeting of enzyme condensates to focal adhesions play a role in regulating cell motility.

### GIT/PIX Condensates Regulate Neuronal Synapse Formation

In addition to focal adhesions, GIT/PIX complexes are found in other cellular locations, such as intracellular vesicles, neuronal synapses, centrioles, cell-cell junctions, and DNA damage repair foci, where they regulate diverse cellular functions (Frank and Hansen, 2008; Zhou et al., 2016). Because there are several protein-protein binding domains or motifs in both proteins, we hypothesized that GIT and PIX may use these domains or motifs to interact with various cellular proteins, which, in turn, can target GIT/PIX condensates to distinct cellular sites. For example, Scribble, a component of the Scribble/Lgl/Dlg master cell polarity regulatory complex (Bilder et al., 2000), can bind to and position  $\beta$ -Pix to specific subdomains in polarized cells (Audebert et al., 2004; Dow et al., 2007). Scribble contains a leucine-rich repeat (LRR) domain and four PDZ domains. The three N-terminal PDZ domains can bind to the PDZ-binding motif (PBM) of  $\beta$ -Pix with micromolar affinities (Lim et al., 2017; Figure 6A). In neurons, Shank family scaffold proteins can use their PDZ domains to bind to  $\beta$ -Pix and, thus, concentrate  $\beta$ -Pix to postsynaptic densities (PSDs) of excitatory synapses for Rac-dependent dendritic spine dynamic modulations (Park et al., 2003; Figure 6A).

We used a sedimentation-based assay to test whether Scribble and Shank can be enriched in GIT1/ $\beta$ -Pix condensates. We used purified Scribble PDZ1-4 for this assay because the protein behaves well (e.g., it is highly soluble and non-aggregating, suitable for quantifying condensed phase formation dur-

ing phase separation). The Shank3 protein used in the assay contains PDZ-HBS-CBS-SAM, as described previously (Zeng et al., 2018). For simplicity, here we refer to these two proteins as Scribble and Shank3. When mixing Scribble or Shank3 with GIT1 and  $\beta$ -Pix at a 1:1:1 molar ratio (the concentration of each protein was 5  $\mu$ M), Scribble or Shank3 was readily recovered from the condensed phase (Figure 6B), indicating that both proteins can be recruited and enriched into GIT1/ $\beta$ -Pix condensates. As we observed with Paxillin (Figure 5D), Scribble and Shank3 can promote phase separation of the GIT1/ $\beta$ -Pix complex (Figure 6B).

In a fluorescence imaging assay, iFluo405-Shank3 coalesced into micrometer-sized GIT1/ $\beta$ -Pix condensates (Figure S8A). Furthermore, the GIT1/ $\beta$ -Pix complex could be integrated into excitatory PSD condensates reconstituted with PSD-95, GKAP, Shank3, SynGAP, NR2B, and Homer at low micromolar concentrations of each protein (i.e., the 6 $\times$  PSD assembly in our earlier study; Zeng et al., 2018; Figure 6C). Formation of the resulting 8-component condensates is specific because addition of the Paxillin LD4 peptide to the system did not affect phase separation of these synaptic proteins (Figure S8B). Importantly, when  $\beta$ -Pix (the link between GIT1 and the PSD components) was dropped out in the 8 $\times$  PSD mixture, GIT1 could still form condensates, but the formed condensates no longer overlapped with the 6 $\times$  PSD condensates (Figure 6D). Moreover, the GIT1/ $\beta$ -Pix<sup>APBM</sup> condensates (the  $\beta$ -Pix<sup>APBM</sup> mutant with removal of the last 4 residues cannot bind to Shank3 but can still bind to GIT1) did not overlap with the 6 $\times$  PSD condensates either (Figures 6E and S8C). The above results indicate that the specific Shank3/ $\beta$ -Pix interaction is required for recruitment of GIT1/ $\beta$ -Pix condensates to PSD condensates (i.e., Shank3 functions as the adaptor for targeting GIT1/ $\beta$ -Pix to PSD condensates). The above finding also indicates that different biological condensates can be brought together or separated by modulating their interactions.

We next investigated whether phase separation of the GIT1/ $\beta$ -Pix complex is required for its synaptic targeting and function. In cultured hippocampal neurons, the expressed GFP- $\beta$ -Pix\_WT showed prominent spine localization, whereas the phase separation-deficient mutant of  $\beta$ -Pix,  $\beta$ -Pix\_VD, which retains its binding to GIT1 and Shank3 but is a monomer (Figures 4D–F), had a

(D) Fluorescence images showing that GIT1 condensates did not overlap with the 6 $\times$  PSD condensates when  $\beta$ -Pix was dropped out of the system (see the experimental scheme below the images).

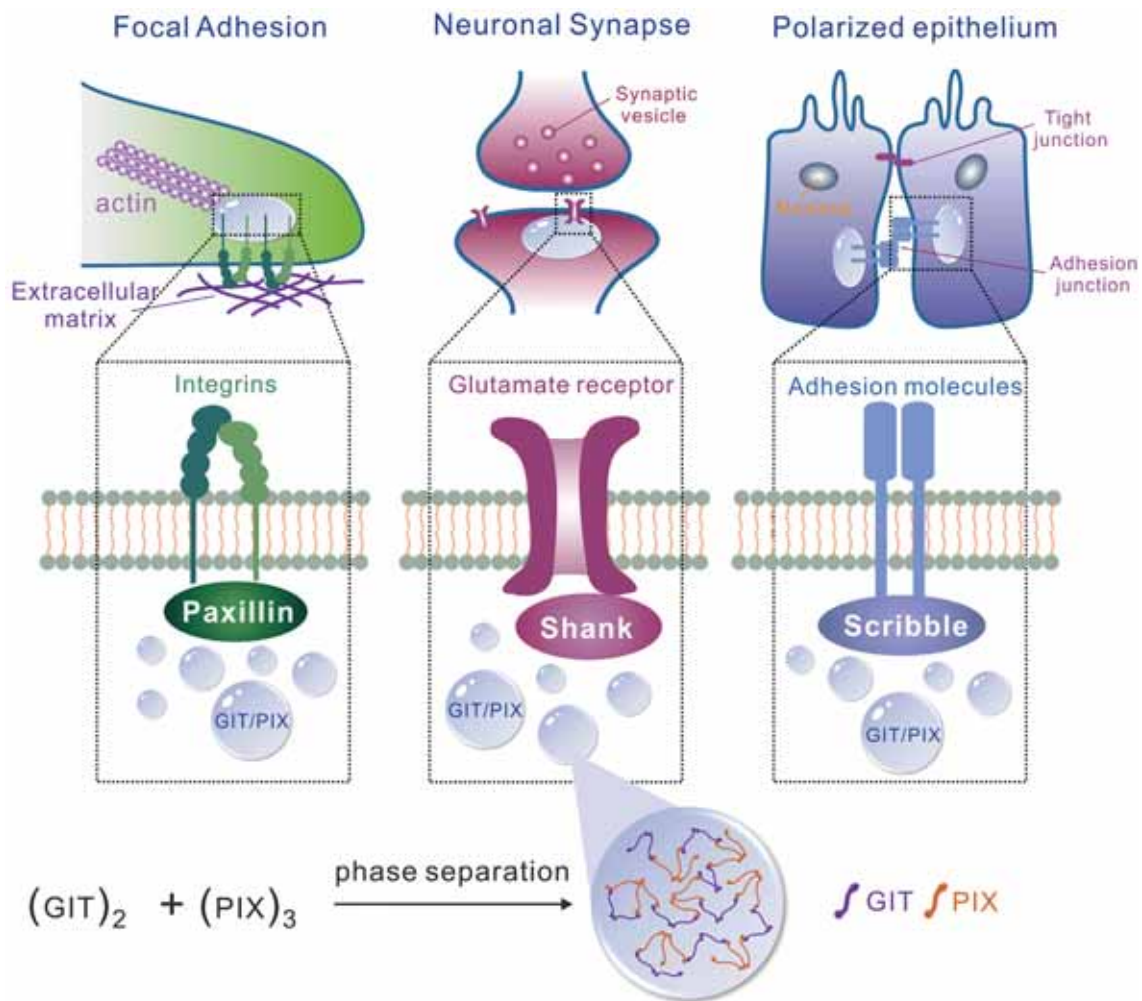
(E) Fluorescence images showing that GIT1/ $\beta$ -Pix<sup>APBM</sup> condensates did not overlap with the 6 $\times$  PSD condensates.  $\beta$ -Pix\* in the experimental scheme below the images represents  $\beta$ -Pix<sup>APBM</sup>.

(F and I) Cultured hippocampal neurons were transfected with GFP-tagged  $\beta$ -Pix constructs (GFP- $\beta$ -Pix\_WT, GFP- $\beta$ -Pix\_VD, and GFP control) (F) or GFP-tagged GIT1 constructs (GIT1\_WT-GFP, GIT1\_LP-GFP, and GFP control) (I) at 14 days in vitro (DIV). mCherry was co-transfected with these constructs as the cell fill. After 4 days of expression, neurons were fixed and mounted for imaging. GFP- $\beta$ -Pix\_WT (F) or GIT1\_WT-GFP (I) showed prominent spine localization, whereas the phase separation-deficient  $\beta$ -Pix\_VD (F) or GIT1\_LP-GFP (I) had a diffused distribution pattern with no significant synaptic enrichment. Notably, compared with the WT and GFP control group, neurons expressing  $\beta$ -Pix\_VD (F) or the GIT1\_LP (I) mutant showed a severe reduction in the proportion of mature spines.

(G and J) Quantification of the imaging data, showing synaptic targeting of various  $\beta$ -Pix (G) or GIT1 (J) constructs. The synaptic enrichment ratio of  $\beta$ -Pix (G) or GIT1 (J) is defined as  $[GFP_{spine}/GFP_{shaft}]/[mCherry_{spine}/mCherry_{shaft}]$ . Eight neurons from three independent batches of cultures were imaged for each group, and each neuron was analyzed for four branches (i.e.,  $n = 32$ ). Error bars indicate  $\pm$  SEM. \*\*\*\* $p < 0.0001$ . One-way ANOVA with Tukey's multiple comparisons test was used for the plot.

(H and K) Quantification of image data, showing a reduction of mature spines for neurons expressing the  $\beta$ -Pix\_VD (H) or GIT1 (K) mutant. Eight neurons from three independent batches of cultures were imaged for each group for quantification. Error bars indicate  $\pm$  SEM. \*\* $p < 0.01$ , \*\*\* $p < 0.001$  One-way ANOVA with Tukey's multiple comparisons test.

See also Figure S8.



## Modular nature of GIT/PIX condensates in various cellular processes

**Figure 7. The Versatile Modular GIT/PIX Condensates Function in Diverse Cellular Processes**

Shown is a model depicting that the GIT/PIX condensates function as a modular organization capable of being targeted to distinct cellular compartments, such as focal adhesions, neuronal synapses, and cell-cell junctions, enabling spatiotemporal regulation of GTPase activities. The GIT/PIX condensates are formed by strong, specific, and multivalent interactions between these two enzymes without additional scaffolding molecules.

diffused distribution pattern with no significant synaptic enrichment (Figures 6F and 6G). Notably, compared with WT  $\beta$ -Pix and the GFP control, neurons expressing  $\beta$ -PIX<sub>VD</sub> showed a severe reduction in mature spines (Figures 6F and 6H). Similarly, in neurons expressing WT GIT1-GFP, GIT1 was enriched into punctum-like structure in dendritic spines, whereas the phase separation-deficient mutant of GIT1, GIT1<sub>LP</sub>, had very limited spine enrichment (Figures 6I and 6J). Like  $\beta$ -Pix<sub>VD</sub>-expressing neurons, neurons expressing GIT1<sub>LP</sub> exhibited a significantly decreased portion of mature spines (Figures 6I and 6K). It should be emphasized that neither the  $\beta$ -Pix<sub>VD</sub> mutant nor the GIT1<sub>LP</sub> mutant directly affects binding between GIT and  $\beta$ -Pix; thus, the mutants were used to specifically probe the role of phase separation of the complex in synaptic targeting and synapse formation. Taken together, the data in Figure 6 indi-

cate that GIT1/ $\beta$ -Pix condensates are recruited to synapses, likely via the  $\beta$ -Pix/Shank3 interaction, and that phase separation of the GIT1/ $\beta$ -Pix complex is crucial for synaptic targeting and dendritic spine development in hippocampal neurons.

### DISCUSSION

In this study, we made two unexpected findings with general implications for cell biology. First, our study reveals that enzymes by themselves (in this case, two small GTPase regulatory enzymes, GIT1 and  $\beta$ -Pix) can form highly specific condensates via phase separation *in vitro* and in living cells. Importantly, formation of GIT1/ $\beta$ -Pix condensates does not require additional scaffold proteins or scaffold-like molecules, such as RNA and DNA, which are often essential for liquid-liquid phase separation

in most of the currently known biological condensate systems (Ditlev et al., 2018; Du and Chen, 2018; Jain and Vale, 2017). Enzymes are generally efficient catalysts and, therefore, do not exist at high concentrations in cells. However, enzymes are known to be concentrated at specific subcellular compartments to perform spatially defined cellular functions. Via liquid-liquid phase separation, enzymes such as GIT1 and  $\beta$ -Pix can autonomously form highly concentrated molecular assemblies, providing a novel mechanism for enriching limited amounts of enzymes into specific cellular regions for fast and spatially defined catalysis (Jang et al., 2019; Webb et al., 2017). Guided by the atomic structures of GIT1,  $\beta$ -Pix, and the GIT/ $\beta$ -Pix complex, we also demonstrated that phase separation-mediated GIT1/ $\beta$ -Pix complex condensation, instead of the classical binary interaction between GIT1 and  $\beta$ -Pix, is required for the enzyme complex to modulate cell migration and synapse formation. It should be noted that formation of large enzyme complexes for certain defined cellular functions via classical stoichiometric interactions (e.g., locally concentrated metabolic enzyme complexes) has been known for decades (Srere, 1987). Our study provides another paradigm to show that concentrated enzyme complex condensates can form via phase separation. Phase separation-mediated formation of dense enzyme complex condensates will likely have distinct properties regarding aspects such as enzyme kinetics, substrate accessibility, threshold concentration, and regulation of enzyme assembly formation. All of these will need to be addressed in future investigations.

Second, our study demonstrates that GIT1/ $\beta$ -Pix condensates can function as a highly concentrated module capable of being recruited to diverse cellular signaling compartments by binding to specific adaptor proteins, such as Paxillin, Scribble, and Shank3 (Figure 7). With this modular feature, GIT1/ $\beta$ -Pix condensates can be specifically recruited to distinct subcellular compartments by different adaptors to perform multiple cellular functions. The modular feature of GIT1/ $\beta$ -Pix condensates for targeting the enzyme complex to different cellular processes is, in a way, analogous to the protein module-based organization of cellular signal transduction pathways. We suggest that formation of such modular regulatory enzyme condensates via phase separation may be a common mechanism for cells to utilize limited amounts of enzymes for broad and optimal cellular function.

In contrast to most of biomolecular condensates reported in the literature, formation of GIT/ $\beta$ -Pix condensates requires a very specific and strong interaction between these two proteins ( $K_D$ ,  $\sim 20$  nM). Such specific interaction is presumably in accordance with the specific functional roles of the two enzymes in various cellular processes. We argue that strong and specific multivalent interactions are critical for forming functionally specific biomolecular condensates in living cells, as we have demonstrated here and also previously in neuronal synapses (Zeng et al., 2016, 2018). Numerous studies in the past have illustrated the critical roles played by weak and multivalent interactions in phase separation of biomolecules. Nonetheless, it is hard to envisage that formation of functionally specific biological signaling condensates is predominantly dictated by promiscuous biomolecular interactions. It is also puzzling how genetic

mutations that only lead to mild changes in binding can cause human diseases, particularly when considering that the interactions involved are weak and promiscuous. We propose that strong and specific interactions, together with weak but often multivalent bindings, allow formation of highly specific biomolecular condensates. These assemblies may have very low phase separation concentration thresholds and broad dynamic properties (Fujioka et al., 2020). For this reason, we recommend use of full-length proteins each at their physiological concentrations to investigate biomolecular condensates formation whenever possible. Much remains to be uncovered in the exciting and emerging field of phase separation-induced membrane-less biomolecular condensates formation.

## STAR★METHODS

Detailed methods are provided in the online version of this paper and include the following:

- KEY RESOURCES TABLE
- RESOURCE AVAILABILITY
  - Lead Contact
  - Materials Availability
  - Data and Code Availability
- EXPERIMENTAL MODEL AND SUBJECT DETAILS
  - Bacterial strain
  - Cell Culture
- METHOD DETAILS
  - Constructs and peptides
  - Protein expression and purification
  - Isothermal titration calorimetry (ITC) assay
  - GST-pull down assay
  - Fast protein liquid chromatography (FPLC) coupled with static light scattering
  - Fluorescence polarization assay
  - Crystallization, Data collection and Structure determination
  - Protein labeling with fluorophore
  - In vitro phase transition assay
  - Fluorescence recovery after photo-bleaching assay
  - HeLa cell imaging, focal adhesion localization and cell migration
  - Primary hippocampal neuron culture and imaging
- QUANTIFICATION AND STATISTICAL ANALYSIS

## SUPPLEMENTAL INFORMATION

Supplemental Information can be found online at <https://doi.org/10.1016/j.molcel.2020.07.004>.

## ACKNOWLEDGMENTS

We thank Shanghai Synchrotron Radiation Facility (SSRF, China) BL19U1 for X-ray beam time; the staff members of the Large-Scale Protein Preparation System and Molecular Imaging System at the National Facility for Protein Science in Shanghai (NFPS), Zhangjiang Lab, China for providing technical support and assistance with data collection and analysis; Yuan Shang (University of Arizona, USA) for help during structure determination; Wenyu Wen (Fudan University, China) for providing assistance with the fluorescence polarization assay; and Jinchuan Zhou for critical reading of the manuscript. This work

was supported by grants from the National Key R&D Program of China (2018YFA0507900 to J.Z., 2019YFA0508402 to M.Z., and 2017YFA0504901 to R.Z.), a grant from the National Natural Science Foundation of China (31770779 to J.Z.), a grant from the Chief Scientist Program of Shanghai Institutes for Biological Sciences, Chinese Academy of Sciences (to R.Z.), and grants from RGC of Hong Kong (AoE-M09-12 and C6004-17G to M.Z.) M.Z. is a Kerry Holdings Professor in Science, a Croucher Foundation Senior Fellow, and a Senior Fellow of IAS at HKUST.

#### AUTHOR CONTRIBUTIONS

J.Z., Q.Z., and M.Z. designed the study. J.Z., Q.Z., Y.X., and M.P. performed the experiments. Y.X., M.P., L.L., and J.L. carried out X-ray data collection and structure determination. J.Z., Q.Z., Y.X., L.L., J.L., R.Z., and M.Z. analyzed the data. J.Z., Q.Z., and M.Z. drafted the manuscript. J.Z. and M.Z. coordinated the project. All authors approved the final version of the manuscript.

#### DECLARATION OF INTERESTS

The authors declare no competing interests.

Received: February 14, 2020

Revised: June 2, 2020

Accepted: July 3, 2020

Published: August 10, 2020

#### REFERENCES

Adams, P.D., Afonine, P.V., Bunkóczi, G., Chen, V.B., Davis, I.W., Echols, N., Headd, J.J., Hung, L.W., Kapral, G.J., Grosse-Kunstleve, R.W., et al. (2010). PHENIX: a comprehensive Python-based system for macromolecular structure solution. *Acta Crystallogr. D Biol. Crystallogr.* **66**, 213–221.

Audebert, S., Navarro, C., Nourry, C., Chasserot-Golaz, S., Lécine, P., Bellaiche, Y., Dupont, J.L., Premont, R.T., Sempéré, C., Strub, J.M., et al. (2004). Mammalian Scribble forms a tight complex with the betaPIX exchange factor. *Curr. Biol.* **14**, 987–995.

Bai, M., Pang, X., Lou, J., Zhou, Q., Zhang, K., Ma, J., Li, J., Sun, F., and Hsu, V.W. (2012). Mechanistic insights into regulated cargo binding by ACAP1 protein. *J. Biol. Chem.* **287**, 28675–28685.

Banani, S.F., Lee, H.O., Hyman, A.A., and Rosen, M.K. (2017). Biomolecular condensates: organizers of cellular biochemistry. *Nat. Rev. Mol. Cell Biol.* **18**, 285–298.

Banjade, S., and Rosen, M.K. (2014). Phase transitions of multivalent proteins can promote clustering of membrane receptors. *eLife* **3**, e04123.

Bilder, D., Li, M., and Perrimon, N. (2000). Cooperative regulation of cell polarity and growth by *Drosophila* tumor suppressors. *Science* **289**, 113–116.

Brangwynne, C.P., Eckmann, C.R., Courson, D.S., Rybarska, A., Hoege, C., Gharakhani, J., Jülicher, F., and Hyman, A.A. (2009). Germline P granules are liquid droplets that localize by controlled dissolution/condensation. *Science* **324**, 1729–1732.

Brangwynne, C.P., Mitchison, T.J., and Hyman, A.A. (2011). Active liquid-like behavior of nucleoli determines their size and shape in *Xenopus laevis* oocytes. *Proc. Natl. Acad. Sci. USA* **108**, 4334–4339.

Chang, D., Gao, F., Slavney, A., Ma, L., Waldman, Y.Y., Sams, A.J., Billing-Ross, P., Madar, A., Spritz, R., and Keinan, A. (2014). Accounting for eXcentricities: analysis of the X chromosome in GWAS reveals X-linked genes implicated in autoimmune diseases. *PLoS ONE* **9**, e113684.

Chen, X., Wu, X., Wu, H., and Zhang, M. (2020). Phase separation at the synapse. *Nat. Neurosci.* **23**, 301–310.

Choi, J.M., Holehouse, A.S., and Pappu, R.V. (2020). Physical Principles Underlying the Complex Biology of Intracellular Phase Transitions. *Annu. Rev. Biophys.* **49**, 107–133.

Chong, S., Dugast-Darzacq, C., Liu, Z., Dong, P., Dailey, G.M., Cattoglio, C., Heckert, A., Banala, S., Lavis, L., Darzacq, X., and Tjian, R. (2018). Imaging dy-

namic and selective low-complexity domain interactions that control gene transcription. *Science* **361**, eaar2555.

Ditlev, J.A., Case, L.B., and Rosen, M.K. (2018). Who's In and Who's Out-Compositional Control of Biomolecular Condensates. *J. Mol. Biol.* **430**, 4666–4684.

Dow, L.E., Kauffman, J.S., Caddy, J., Zarbalis, K., Peterson, A.S., Jane, S.M., Russell, S.M., and Humbert, P.O. (2007). The tumour-suppressor Scribble dictates cell polarity during directed epithelial migration: regulation of Rho GTPase recruitment to the leading edge. *Oncogene* **26**, 2272–2282.

Du, M., and Chen, Z.J. (2018). DNA-induced liquid phase condensation of cGAS activates innate immune signaling. *Science* **361**, 704–709.

Emsley, P., and Cowtan, K. (2004). Coot: model-building tools for molecular graphics. *Acta Crystallogr. D Biol. Crystallogr.* **60**, 2126–2132.

Feng, Q., Baird, D., Peng, X., Wang, J., Ly, T., Guan, J.L., and Cerione, R.A. (2006). Cool-1 functions as an essential regulatory node for EGF receptor- and Src-mediated cell growth. *Nat. Cell Biol.* **8**, 945–956.

Feng, Z., Chen, X., Wu, X., and Zhang, M. (2019). Formation of biological condensates via phase separation: Characteristics, analytical methods, and physiological implications. *J. Biol. Chem.* **294**, 14823–14835.

Frank, S.R., and Hansen, S.H. (2008). The PIX-GIT complex: a G protein signaling cassette in control of cell shape. *Semin. Cell Dev. Biol.* **19**, 234–244.

Fujioka, Y., Alam, J.M., Noshiro, D., Mouri, K., Ando, T., Okada, Y., May, A.I., Knorr, R.L., Suzuki, K., Ohsumi, Y., and Noda, N.N. (2020). Phase separation organizes the site of autophagosome formation. *Nature* **578**, 301–305.

Hoefen, R.J., and Berk, B.C. (2006). The multifunctional GIT family of proteins. *J. Cell Sci.* **119**, 1469–1475.

Hoellerer, M.K., Noble, M.E., Labesse, G., Campbell, I.D., Werner, J.M., and Arold, S.T. (2003). Molecular recognition of paxillin LD motifs by the focal adhesion targeting domain. *Structure* **11**, 1207–1217.

Hyman, A.A., Weber, C.A., and Jülicher, F. (2014). Liquid-liquid phase separation in biology. *Annu. Rev. Cell Dev. Biol.* **30**, 39–58.

Ismail, S.A., Vetter, I.R., Sot, B., and Wittinghofer, A. (2010). The structure of an Arf-ArfGAP complex reveals a Ca<sup>2+</sup> regulatory mechanism. *Cell* **141**, 812–821.

Jain, A., and Vale, R.D. (2017). RNA phase transitions in repeat expansion disorders. *Nature* **546**, 243–247.

Jang, S., Xuan, Z., Lagoy, R.C., Jawerth, L.M., Gonzalez, I., Singh, M., Prashad, S., Kim, H.S., Patel, A., Albrecht, D.R., et al. (2019). The Glycolytic Protein Phosphofructokinase Dynamically Relocalizes into Subcellular Compartments with Liquid-like Properties in vivo. *bioRxiv*. <https://doi.org/10.1101/636449>.

Kutsche, K., Yntema, H., Brandt, A., Jantke, I., Nothwang, H.G., Orth, U., Boavida, M.G., David, D., Chelly, J., Fryns, J.P., et al. (2000). Mutations in ARHGEF6, encoding a guanine nucleotide exchange factor for Rho GTPases, in patients with X-linked mental retardation. *Nat. Genet.* **26**, 247–250.

Li, X., Ji, W., Zhang, R., Folta-Stogniew, E., Min, W., and Boggon, T.J. (2011). Molecular recognition of leucine-aspartate repeat (LD) motifs by the focal adhesion targeting homology domain of cerebral cavernous malformation 3 (CCM3). *J. Biol. Chem.* **286**, 26138–26147.

Li, P., Banjade, S., Cheng, H.C., Kim, S., Chen, B., Guo, L., Llaguno, M., Hollingsworth, J.V., King, D.S., Banani, S.F., et al. (2012). Phase transitions in the assembly of multivalent signalling proteins. *Nature* **483**, 336–340.

Lim, K.Y.B., Gödde, N.J., Humbert, P.O., and Kvasnakul, M. (2017). Structural basis for the differential interaction of Scribble PDZ domains with the guanine nucleotide exchange factor  $\beta$ -PIX. *J. Biol. Chem.* **292**, 20425–20436.

Mandiyan, V., Andreev, J., Schlessinger, J., and Hubbard, S.R. (1999). Crystal structure of the ARF-GAP domain and ankyrin repeats of PYK2-associated protein beta. *EMBO J.* **18**, 6890–6898.

Manser, E., Loo, T.H., Koh, C.G., Zhao, Z.S., Chen, X.Q., Tan, L., Tan, I., Leung, T., and Lim, L. (1998). PAK kinases are directly coupled to the PIX family of nucleotide exchange factors. *Mol. Cell* **1**, 183–192.

- Mayhew, M.W., Jeffery, E.D., Sherman, N.E., Nelson, K., Polefrone, J.M., Pratt, S.J., Shabanowitz, J., Parsons, J.T., Fox, J.W., Hunt, D.F., and Horwitz, A.F. (2007). Identification of phosphorylation sites in betaPIX and PAK1. *J. Cell Sci.* *120*, 3911–3918.
- McCoy, A.J., Grosse-Kunstleve, R.W., Adams, P.D., Winn, M.D., Storoni, L.C., and Read, R.J. (2007). Phaser crystallographic software. *J. Appl. Cryst.* *40*, 658–674.
- Minor, W., Cymborowski, M., Otwinowski, Z., and Chruszcz, M. (2006). HKL-3000: the integration of data reduction and structure solution—from diffraction images to an initial model in minutes. *Acta Crystallogr. D Biol. Crystallogr.* *62*, 859–866.
- Molliex, A., Temirov, J., Lee, J., Coughlin, M., Kanagaraj, A.P., Kim, H.J., Mittag, T., and Taylor, J.P. (2015). Phase separation by low complexity domains promotes stress granule assembly and drives pathological fibrillization. *Cell* *163*, 123–133.
- Park, E., Na, M., Choi, J., Kim, S., Lee, J.R., Yoon, J., Park, D., Sheng, M., and Kim, E. (2003). The Shank family of postsynaptic density proteins interacts with and promotes synaptic accumulation of the beta PIX guanine nucleotide exchange factor for Rac1 and Cdc42. *J. Biol. Chem.* *278*, 19220–19229.
- Patel, A., Lee, H.O., Jawerth, L., Maharana, S., Jahnel, M., Hein, M.Y., Stoynev, S., Mahamid, J., Saha, S., Franzmann, T.M., et al. (2015). A Liquid-to-Solid Phase Transition of the ALS Protein FUS Accelerated by Disease Mutation. *Cell* *162*, 1066–1077.
- Peng, H., Dara, L., Li, T.W., Zheng, Y., Yang, H., Tomasi, M.L., Tomasi, I., Giordano, P., Mato, J.M., and Lu, S.C. (2013). MAT2B-GIT1 interplay activates MEK1/ERK 1 and 2 to induce growth in human liver and colon cancer. *Hepatology* *57*, 2299–2313.
- Premont, R.T., Claing, A., Vitale, N., Freeman, J.L., Pitcher, J.A., Patton, W.A., Moss, J., Vaughan, M., and Lefkowitz, R.J. (1998). beta2-Adrenergic receptor regulation by GIT1, a G protein-coupled receptor kinase-associated ADP-ribosylation factor GTPase-activating protein. *Proc. Natl. Acad. Sci. USA* *95*, 14082–14087.
- Premont, R.T., Claing, A., Vitale, N., Perry, S.J., and Lefkowitz, R.J. (2000). The GIT family of ADP-ribosylation factor GTPase-activating proteins. Functional diversity of GIT2 through alternative splicing. *J. Biol. Chem.* *275*, 22373–22380.
- Premont, R.T., Perry, S.J., Schmalzigaug, R., Roseman, J.T., Xing, Y., and Claing, A. (2004). The GIT/PIX complex: an oligomeric assembly of GIT family ARF GTPase-activating proteins and PIX family Rac1/Cdc42 guanine nucleotide exchange factors. *Cell. Signal.* *16*, 1001–1011.
- Sabari, B.R., Dall'Agnesse, A., Boija, A., Klein, I.A., Coffey, E.L., Shrinivas, K., Abraham, B.J., Hannett, N.M., Zamudio, A.V., Manteiga, J.C., et al. (2018). Coactivator condensation at super-enhancers links phase separation and gene control. *Science* *361*, eaar3958.
- Schlenker, O., and Rittinger, K. (2009). Structures of dimeric GIT1 and trimeric beta-PIX and implications for GIT-PIX complex assembly. *J. Mol. Biol.* *386*, 280–289.
- Schmalzigaug, R., Garron, M.L., Roseman, J.T., Xing, Y., Davidson, C.E., Arold, S.T., and Premont, R.T. (2007). GIT1 utilizes a focal adhesion targeting-homology domain to bind paxillin. *Cell. Signal.* *19*, 1733–1744.
- Shan, Z., Tu, Y., Yang, Y., Liu, Z., Zeng, M., Xu, H., Long, J., Zhang, M., Cai, Y., and Wen, W. (2018). Basal condensation of Numb and Pon complex via phase transition during *Drosophila* neuroblast asymmetric division. *Nat. Commun.* *9*, 737.
- Shin, Y., and Brangwynne, C.P. (2017). Liquid phase condensation in cell physiology and disease. *Science* *357*, eaaf4382.
- Srere, P.A. (1987). Complexes of sequential metabolic enzymes. *Annu. Rev. Biochem.* *56*, 89–124.
- Turner, C.E., Brown, M.C., Perrotta, J.A., Riedy, M.C., Nikolopoulos, S.N., McDonald, A.R., Bagrodia, S., Thomas, S., and Leventhal, P.S. (1999). Paxillin LD4 motif binds PAK and PIX through a novel 95-kD ankyrin repeat, ARF-GAP protein: A role in cytoskeletal remodeling. *J. Cell Biol.* *145*, 851–863.
- Vanarotti, M.S., Miller, D.J., Guibao, C.D., Nourse, A., and Zheng, J.J. (2014). Structural and mechanistic insights into the interaction between Pyk2 and paxillin LD motifs. *J. Mol. Biol.* *426*, 3985–4001.
- Vitale, N., Patton, W.A., Moss, J., Vaughan, M., Lefkowitz, R.J., and Premont, R.T. (2000). GIT proteins, A novel family of phosphatidylinositol 3,4,5-trisphosphate-stimulated GTPase-activating proteins for ARF6. *J. Biol. Chem.* *275*, 13901–13906.
- Wang, J., Choi, J.M., Holehouse, A.S., Lee, H.O., Zhang, X., Jahnel, M., Maharana, S., Lemaitre, R., Pozniakovsky, A., Drechsel, D., et al. (2018). A Molecular Grammar Governing the Driving Forces for Phase Separation of Prion-like RNA Binding Proteins. *Cell* *174*, 688–699.e16.
- Webb, B.A., Dosey, A.M., Wittmann, T., Kollman, J.M., and Barber, D.L. (2017). The glycolytic enzyme phosphofructokinase-1 assembles into filaments. *J. Cell Biol.* *216*, 2305–2313.
- Won, H., Mah, W., Kim, E., Kim, J.W., Hahn, E.K., Kim, M.H., Cho, S., Kim, J., Jang, H., Cho, S.C., et al. (2011). GIT1 is associated with ADHD in humans and ADHD-like behaviors in mice. *Nat. Med.* *17*, 566–572.
- Woodruff, J.B., Wueseke, O., Viscardi, V., Mahamid, J., Ochoa, S.D., Bunkenborg, J., Widlund, P.O., Pozniakovsky, A., Zanin, E., Bahmanyar, S., et al. (2015). Centrosomes. Regulated assembly of a supramolecular centrosome scaffold in vitro. *Science* *348*, 808–812.
- Woodruff, J.B., Ferreira Gomes, B., Widlund, P.O., Mahamid, J., Honigsmann, A., and Hyman, A.A. (2017). The Centrosome Is a Selective Condensate that Nucleates Microtubules by Concentrating Tubulin. *Cell* *169*, 1066–1077.e10.
- Wright, P.E., and Dyson, H.J. (2015). Intrinsically disordered proteins in cellular signalling and regulation. *Nat. Rev. Mol. Cell Biol.* *16*, 18–29.
- Wu, X., Cai, Q., Shen, Z., Chen, X., Zeng, M., Du, S., and Zhang, M. (2019). RIM and RIM-BP Form Presynaptic Active-Zone-like Condensates via Phase Separation. *Mol. Cell* *73*, 971–984.e5.
- Zeng, M., Shang, Y., Araki, Y., Guo, T., Haganir, R.L., and Zhang, M. (2016). Phase Transition in Postsynaptic Densities Underlies Formation of Synaptic Complexes and Synaptic Plasticity. *Cell* *166*, 1163–1175.e12.
- Zeng, M., Chen, X., Guan, D., Xu, J., Wu, H., Tong, P., and Zhang, M. (2018). Reconstituted Postsynaptic Density as a Molecular Platform for Understanding Synapse Formation and Plasticity. *Cell* *174*, 1172–1187.e16.
- Zeng, M., Diaz-Alonso, J., Ye, F., Chen, X., Xu, J., Ji, Z., Nicoll, R.A., and Zhang, M. (2019). Phase Separation-Mediated TARP/MAGUK Complex Condensation and AMPA Receptor Synaptic Transmission. *Neuron* *104*, 529–543.e6.
- Zhang, Z.M., Simmerman, J.A., Guibao, C.D., and Zheng, J.J. (2008). GIT1 paxillin-binding domain is a four-helix bundle, and it binds to both paxillin LD2 and LD4 motifs. *J. Biol. Chem.* *283*, 18685–18693.
- Zhao, Z.S., Manser, E., Loo, T.H., and Lim, L. (2000). Coupling of PAK-interacting exchange factor PIX to GIT1 promotes focal complex disassembly. *Mol. Cell. Biol.* *20*, 6354–6363.
- Zhou, W., Li, X., and Premont, R.T. (2016). Expanding functions of GIT Arf GTPase-activating proteins, PIX Rho guanine nucleotide exchange factors and GIT-PIX complexes. *J. Cell Sci.* *129*, 1963–1974.
- Zhu, J., Zhou, Q., Shang, Y., Li, H., Peng, M., Ke, X., Weng, Z., Zhang, R., Huang, X., Li, S.S.C., et al. (2017). Synaptic Targeting and Function of SAPAPs Mediated by Phosphorylation-Dependent Binding to PSD-95 MAGUKs. *Cell Rep.* *21*, 3781–3793.

STAR★METHODS

KEY RESOURCES TABLE

REAGENT or RESOURCE	SOURCE	IDENTIFIER
<b>Antibodies</b>		
Anti-Flag antibody	Sigma-Aldrich	Cat# F1804
Anti-Paxillin antibody	BD Biosciences	Cat# 554002
Anti-β-Pix antibody	Millipore Sigma	Cat# 07-1450-I
Anti-Myc antibody	DSHB	Cat# 9E-10
Anti-Vinculin antibody	Sigma-Aldrich	Cat#V9131
Alexa Fluor 647 donkey anti-mouse	Thermo Fisher	Cat# A31571
Alexa Fluor 594 donkey anti-rabbit	Thermo Fisher	Cat# A21207
<b>Bacterial and Virus Strains</b>		
<i>Escherichia coli</i> BL21 (DE3)	TRANSGEN BIOTECH	Cat# CD601
<i>Escherichia coli</i> BL21 (Codon Plus)	Agilent	Cat# 230240
<b>Chemicals, Peptides, and Recombinant Proteins</b>		
Dulbecco's Modified Eagle Medium (DMEM)	Thermo Fisher	Cat# 11995065
Fetal bovine serum (FBS)	Thermo Fisher	Cat# 16000044
Alexa Fluor 488 NHS ester	Thermo Fisher	Cat# A20000
Cy3 NHS ester	AAT Bioquest	Cat# 271
Cy5 NHS Ester	AAT Bioquest	Cat# 280
Fluorescein-5-isothiocyanate	Thermo Fisher	Cat# F1907
Recombinant protein: GIT1 full length (aa 1-770)	This paper	N/A
Recombinant protein: GIT1 GAS (aa 1-370)	This paper	N/A
Recombinant protein: GIT1 FAT (aa 640-770)	This paper	N/A
Recombinant protein: GIT1 CC (aa 425-485)	This paper	N/A
Recombinant protein: GIT1 CC_LP (aa 425-485, L438P, L459P, L466P)	This paper	N/A
Recombinant protein: GIT1 _LP (aa 1-770, L438P, L459P, L466P)	This paper	N/A
Recombinant protein: GIT1 SHD (aa 263-730)	This paper	N/A
Recombinant protein: GIT1 GAS-CC (aa 1-485)	This paper	N/A
Recombinant protein: GIT1_del8 (aa 1-770, delete 254-261)	This paper	N/A
Recombinant protein: GIT2 GAS (aa 1-361)	This paper	N/A
Recombinant protein: GIT2 GAS_S255A/S256A	This paper	N/A
Recombinant protein: GIT2 GAS_L273A	This paper	N/A
Recombinant protein: GIT2 GAS_L281A	This paper	N/A
Recombinant protein: GIT2 GAS_D348A	This paper	N/A
Recombinant protein: β-Pix _494-555	This paper	N/A
Recombinant protein: β-Pix GBD (aa 528-548)	This paper	N/A
Recombinant protein: β-Pix GBD_Y542D	This paper	N/A
Recombinant protein: β-Pix GBD_I535D	This paper	N/A
Recombinant protein: β-Pix_528-543	This paper	N/A
Recombinant protein: β-Pix_494-548	This paper	N/A
Recombinant protein: β-Pix_CC (aa 588-646)	This paper	N/A
Recombinant protein: β-Pix_CC_VD (aa 588-646, V601D/V629D)	This paper	N/A
Recombinant protein: β-Pix full length (aa 1-646)	This paper	N/A

(Continued on next page)

**Continued**

REAGENT or RESOURCE	SOURCE	IDENTIFIER
Recombinant protein: $\beta$ -Pix_VD (aa 1-646, V601D/V629D)	This paper	N/A
Recombinant protein: $\beta$ -Pix_Y542D (aa 1-646, Y542D)	This paper	N/A
Recombinant protein: GIT1 FAT-GS-Paxillin LD4 (GIT1 640-770-(GS) <sub>5</sub> -Paxillin 261-282)	This paper	N/A
Recombinant protein: Paxillin full length (aa 1- 591)	This paper	N/A
Recombinant protein: Paxillin LD1 (aa 1- 16)	This paper	N/A
Recombinant protein: Paxillin LD2 (aa 138- 158)	This paper	N/A
Recombinant protein: Paxillin LD3 (aa 210- 234)	This paper	N/A
Recombinant protein: Paxillin LD4 (aa 261- 282)	This paper	N/A
Recombinant protein: Paxillin LD5 (aa 331- 346)	This paper	N/A
Recombinant protein: Shank3 NPZ-HBS-CBS-SAM	<a href="#">Zeng et al., 2018</a>	N/A
Recombinant protein: Scribble PDZ1-4 (aa 715-1196)	This paper	N/A
Peptide: $\beta$ -Pix GBD (ALEEDAQILKVEAYCTSAKT)	This paper	N/A
Peptide: $\beta$ -Pix GBD_Y542D (ALEEDAQILKVEADCTSAKT)	This paper	N/A
Peptide:Paxillin-LD4 (ATREDELMASLSDFKM)	This paper	N/A
<b>Critical Commercial Assays</b>		
Lipofectamine2000 transfection kit	Invitrogen	Cat# 11668019
Viafect	Promega	Cat# E4981
<b>Deposited Data</b>		
Crystal structure of GIT1/Paxillin complex	This paper	PDB code: 6JMT
Crystal structure of GIT2/ $\beta$ -Pix complex	This paper	PDB code: 6JMU
Crystal structure of GIT1 FAT	<a href="#">Zhang et al., 2008</a>	PDB code: 2JX0
Crystal structure of Pyk2/Paxillin LD4 complex	<a href="#">Vanarotti et al., 2014</a>	PDB code: 4R32
Crystal structure of FAK/Paxillin LD4 complex	<a href="#">Hoellerer et al., 2003</a>	PDB code: 1OW6
Crystal structure of CCM3/Paxillin LD4 complex	<a href="#">Li et al., 2011</a>	PDB code: 3RQG
Crystal structure of ACAP1 GAP-ANK	<a href="#">Bai et al., 2012</a>	PDB code: 3JUE
Crystal structure of GIT1 coiled-coil	<a href="#">Schlenker and Rittinger, 2009</a>	PDB code: 2W6A
Crystal structure of $\beta$ -Pix coiled-coil	<a href="#">Schlenker and Rittinger, 2009</a>	PDB code: 2W6B
<b>Experimental Models: Cell Lines</b>		
HEK293T cell line	ATCC	Cat# CRL-3216
HeLa cell line	ATCC	Cat# CCL-2
<b>Recombinant DNA</b>		
Plasmid: pGEX-4T-1- $\beta$ -Pix GBD WT/mutants	This paper	N/A
Plasmid: pGEX-4T-1-GIT2 GAS WT/mutants	This paper	N/A
Plasmid: pGEX-4T-1-GIT1 GAS	This paper	N/A
Plasmid: pET32m3c-GIT1 GAS	This paper	N/A
Plasmid: pET32m3c-GIT2 GAS	This paper	N/A
Plasmid: pET32m3c- $\beta$ -Pix GBD	This paper	N/A
Plasmid: pET32m3c- $\beta$ -Pix_494-555	This paper	N/A
Plasmid: pET32m3c- $\beta$ -Pix_528-543	This paper	N/A
Plasmid: pET32m3c- $\beta$ -Pix_494-548	This paper	N/A
Plasmid: pET32m3c-Shank3 NPZ-HBS-CBS-SAM	<a href="#">Zeng et al., 2018</a>	N/A
Plasmid: pET32m3c-Scribble PDZ1-4	This paper	N/A
Plasmid: pET32m3c-GIT1 FAT-(GS) <sub>5</sub> -Paxillin LD4	This paper	N/A
Plasmid: pET32m3c-GIT1 full length	This paper	N/A
Plasmid: pET32m3c- $\beta$ -Pix full length	This paper	N/A
Plasmid: pET32m3c-Paxillin full length	This paper	N/A
Plasmid: pET32m3c-Paxillin LD1	This paper	N/A

(Continued on next page)

**Continued**

REAGENT or RESOURCE	SOURCE	IDENTIFIER
Plasmid: pET32m3c-Paxillin LD2	This paper	N/A
Plasmid: pET32m3c-Paxillin LD3	This paper	N/A
Plasmid: pET32m3c-Paxillin LD4	This paper	N/A
Plasmid: pET32m3c-Paxillin LD5	This paper	N/A
Plasmid: Flag-GIT2 GAS WT/mutants	This paper	N/A
Plasmid: GIT1-GFP (pEGFP-N1)	This paper	N/A
Plasmid: GIT1_LP-GFP (pEGFP-N1)	This paper	N/A
Plasmid: GIT1_del8-GFP (pEGFP-N1)	This paper	N/A
Plasmid: GFP-GIT1_CTD (aa371-770)	This paper	N/A
Plasmid: RFP- $\beta$ -Pix	This paper	N/A
Plasmid: RFP- $\beta$ -Pix_VD	This paper	N/A
Plasmid: GFP- $\beta$ -Pix (pEGFP-C1)	This paper	N/A
Plasmid: GFP- $\beta$ -Pix_VD (pEGFP-C1)	This paper	N/A
Plasmid: pCMV-Myc- $\beta$ -Pix	This paper	N/A
Plasmid: RFP-Paxillin	This paper	N/A
<b>Software and Algorithms</b>		
HKL3000 package	Minor et al., 2006	<a href="https://www.hkl-xray.com/hkl-3000">https://www.hkl-xray.com/hkl-3000</a>
PHASER	McCoy et al., 2007	<a href="https://www.phaser.cimr.cam.ac.uk/index.php/Phaser_Crystallographic_Software">https://www.phaser.cimr.cam.ac.uk/index.php/Phaser_Crystallographic_Software</a>
PHENIX	Adams et al., 2010	<a href="https://www.phenix-online.org/">https://www.phenix-online.org/</a>
COOT	Emsley and Cowtan, 2004	<a href="https://www2.mrc-lmb.cam.ac.uk/personal/pemsley/coot/">https://www2.mrc-lmb.cam.ac.uk/personal/pemsley/coot/</a>
PyMOL	Molecular Graphics System, Schrodinger, LLC	<a href="https://pymol.org/2/">https://pymol.org/2/</a>
Origin 7.0	Microcal	<a href="https://microcal-origin.software.informer.com/">https://microcal-origin.software.informer.com/</a>
GraphPad Prism	GraphPad Software Inc	<a href="https://www.graphpad.com:443/scientific-software/prism/">https://www.graphpad.com:443/scientific-software/prism/</a>
ImageJ	NIH	<a href="https://imagej.nih.gov/ij/">https://imagej.nih.gov/ij/</a>
ASTRA6	Wyatt	<a href="https://www.wyatt.com/products/software/astra.html">https://www.wyatt.com/products/software/astra.html</a>

**RESOURCE AVAILABILITY**

**Lead Contact**

Further information and requests for reagents may be directed to, and will be fulfilled by the Lead Contact, Dr. Mingjie Zhang ([mzhang@ust.hk](mailto:mzhang@ust.hk)).

**Materials Availability**

Materials such as plasmids will be available without further restrictions upon request to the Lead Contact ([mzhang@ust.hk](mailto:mzhang@ust.hk)).

**Data and Code Availability**

The atomic coordinates of the GIT2/ $\beta$ -Pix and GIT1/Paxillin complexes are deposited to the Protein Data Bank and have been released under the accession codes: 6JMT and 6JMU, respectively. Original imaging data have been deposited to Mendeley data: <https://data.mendeley.com/datasets/wztrr8v7ps/2>. Other data are available from the corresponding author upon reasonable request.

**EXPERIMENTAL MODEL AND SUBJECT DETAILS**

**Bacterial strain**

*Escherichia coli* BL21 (DE3) and (Codon Plus) cells were used in this study for the production of recombinant proteins. Cells were cultured in LB medium supplemented with necessary antibiotics.

### Cell Culture

HeLa and HEK293T cells were both cultured in Dulbecco's Modified Eagle Medium (DMEM) supplemented with 10% fetal bovine serum (FBS). Cultured cells were maintained at 37°C with 5% CO<sub>2</sub>. Cells were tested negative for mycoplasma contamination by cytoplasmic DAPI staining. The cells were not further authenticated.

### METHOD DETAILS

#### Constructs and peptides

Mouse *GIT1* (GenBank: NM\_001004144.1), *GIT2* (GenBank: NM\_001077360.1), *Arhgef7* (encoding  $\beta$ -Pix; GenBank: NM\_017402.5), and *Pxn* (encoding Paxillin; GenBank: NM\_133915.3) genes were amplified from mouse brain cDNA library. Mouse full length *Shank3* gene was kindly provided by Dr. Guoping Feng at Massachusetts Institute of Technology. Human *Scrib* (encoding Scribble; GenBank: NM\_015356.4) gene was amplified from human cDNA library. Various fragments of these genes were amplified by standard PCR method and cloned into pGEX 4T-1, pET32M3C (with a N-terminal Trx-His<sub>6</sub> tag), pEGFP-N1, pEGFP-C1, pTRFP, pCDNA3.1-Flag or pCMV-Myc vector. Mutations were created through site-directed mutagenesis method. All constructs were confirmed by DNA sequencing.

The wild-type  $\beta$ -Pix GBD peptide (sequence: ALEEDAQILKVEAYCTSAKT),  $\beta$ -Pix GBD\_Y542D (sequence: ALEEDAQILKVEADCTSAKT), and Paxillin LD4 peptide (sequence: ATRELDLMASLSDFKM) were commercially synthesized by ChinaPeptides (Shanghai, China) with purity > 95%.

#### Protein expression and purification

Recombinant proteins were expressed in *Escherichia coli* BL21 (DE3) or (Codon Plus) cells at 16°C for 18h inducing by the isopropyl- $\beta$ -D-thiogalactoside (IPTG) at a final concentration of 0.2 mM. The N-terminal Trx-His<sub>6</sub> tagged and GST-tagged proteins were purified by Ni<sup>2+</sup>-NTA agarose affinity chromatography and GSH-Sepharose affinity chromatography, respectively, and followed by a Superdex-200 26/60 size-exclusion chromatography. For  $\beta$ -Pix and Paxillin full length proteins, a step of monoQ column was used to remove nucleic acids contamination or degraded proteins.

#### Isothermal titration calorimetry (ITC) assay

ITC measurements were carried out on a MicroCal VP-ITC system (Malvern) at 25°C. Various *GIT1* (in the cell, ~50  $\mu$ M) and  $\beta$ -Pix (in the syringe, ~500  $\mu$ M) proteins were in the buffer containing 50 mM Tris (pH 8.0), 100 mM NaCl, and 4 mM  $\beta$ -ME. LD motifs of Paxillin (in the syringe, ~500  $\mu$ M) and *GIT1* FAT (in the cell, ~50  $\mu$ M) proteins were in the buffer containing 50 mM Tris, pH 8.0, 100 mM NaCl, 1 mM EDTA and 1 mM DTT. In each titration, 10  $\mu$ L aliquot of protein in the syringe was injected into the cell at a time interval of 120 s make sure that the titration peak returned to the baseline. Titration data were fitted with the one-site binding model using Origin 7.0.

#### GST-pull down assay

Flag-tagged wild-type and mutants of *GIT2* GAS were overexpressed in HEK293T cells. Cells were harvested and lysed by the ice-cold cell lysis buffer (50 mM HEPES pH 7.4, 150 mM NaCl, 10% glycerol, 2 mM MgCl<sub>2</sub>, 1% Triton and protease inhibitor cocktail). After centrifugation at 16,873 g for 10 min at 4°C, the supernatants were incubated with 20  $\mu$ l various wild-type or mutants of GST- $\beta$ -Pix GBD pre-loaded GSH-Sepharose 4B slurry beads. After extensive wash with the cell lysis buffer, the captured proteins were eluted by 20  $\mu$ l 2  $\times$  SDS-PAGE loading dye and detected by western blot using anti-Flag antibody (Sigma, 1:3000, Cat# F1804).

#### Fast protein liquid chromatography (FPLC) coupled with static light scattering

The analysis was performed on an Agilent InfinityLab system coupled with a static light scattering detector (miniDawn, Wyatt) and a differential refractive index detector (Optilab, Wyatt). 150  $\mu$ L *GIT1*-CC or  $\beta$ -Pix-CC protein sample at 50  $\mu$ M was loaded into a Superose 12 10/300 GL column (GE Healthcare) pre-equilibrated with 50 mM Tris, pH 8.0, 100 mM NaCl, 1 mM EDTA, 1 mM DTT buffer. Data were analyzed using ASTRA 6 software (Wyatt).

#### Fluorescence polarization assay

Fluorescence polarization assay was carried out on a PerkinElmer LS-55 fluorimeter equipped with an automated polarizer at 25°C. In the assay, the commercially synthesized WT and mutant  $\beta$ -Pix GBD peptides were labeled with fluorescein-5-isothiocyanate (FITC) (Invitrogen, Molecular Probe) at their N-termini. The FITC-labeled WT or mutant  $\beta$ -Pix GBD peptide was titrated with WT or mutant *GIT2* GAS or *GIT1* GAS in the buffer containing 50 mM Tris, pH 8.0, 100 mM NaCl, 1 mM DTT. The  $K_d$  value was fitted with classical one-site specific binding model using GraphPad Prism.

#### Crystallization, Data collection and Structure determination

##### The *GIT2* GAS/ $\beta$ -Pix GBD complex

For the *GIT2* GAS<sup>S255A/S256A</sup>/ $\beta$ -Pix GBD complex, *GIT2* GAS<sup>S255A/S256A</sup> was mixed with a commercially synthesized  $\beta$ -Pix GBD peptide in a molar ratio of 1:1.3 (~8 mg/ml) in the buffer of 50 mM Tris, pH 8.0, 100 mM NaCl, 2 mM DTT. The best crystals were obtained by the hanging drop diffusion method at 16°C in the buffer condition containing 0.2 M NaF, 0.1 M Bis-Tris propane/citric acid pH 6.7

and 16% PEG3350. Crystals were soaked in crystallization solution containing 25% glycerol for cryo-protection. The diffraction data were collected at BL19U1 at Shanghai Synchrotron Radiation Facility (SSRF, China). The diffraction data were processed with the HKL3000 package (Minor et al., 2006). The complex structure was solved by the molecular replacement method by PHASER (McCoy et al., 2007) using the structure of GAP-ANK tandem of ACAP1 (PDB code: 3JUE) as the searching model. Further refinement was performed using PHENIX (Adams et al., 2010) and Coot (Emsley and Cowtan, 2004). The final refinement statistics of the complex structures were listed in Table S1.

#### The GIT1 FAT/Paxillin LD4 complex

To obtain stable GIT1/Paxillin complex, GIT1 FAT (aa 640-770) was fused with a “GSGSGSGSGS” linker and Paxillin LD4 (aa 261-282). The best crystals of the fusion protein (~20 mg/ml) were obtained by the hanging drop diffusion method at 16°C in the buffer containing 0.2 M (NH<sub>4</sub>)<sub>2</sub>SO<sub>4</sub>, 30% PEG4000. Before X-ray diffraction experiments, crystals were soaked in crystallization solution containing 25% glycerol for cryo-protection. The diffraction data were collected at BL19U1 at Shanghai Synchrotron Radiation Facility (SSRF, China), and processed with the HKL3000 package. Using the structure of the GIT1 FAT apo form structure (PDB code: 2JX0) as the search model, the initial structural model was solved using the molecular replacement method using the software suits of PHASER. Refinements were carried out using PHENIX. The dataset was twinned with a twin fraction of 0.37 as indicated by phenix.xtriage (Adams et al., 2010). Twin refinement restraints were applied during the refinement. Coot was used for Paxillin peptide modeling and model adjustments. The final refinement statistics of the complex structures were listed in Table S1. All structural diagrams were prepared by PyMOL.

#### Protein labeling with fluorophore

Purified proteins were exchanged into the NaHCO<sub>3</sub> buffer containing 300 mM NaCl, 100 mM NaHCO<sub>3</sub>, pH 8.3, 4 mM β-ME using a HiTrap desalting column and concentrated to 5 mg/ml before reaction. Cy3/Cy5 NHS ester (AAT Bioquest) and Alexa 488 NHS ester (Thermo Fisher) were dissolved in DMSO and incubated with the corresponding protein at room temperature for 1h. The fluorophore was mixed with protein solution in 1:1 molar ratio. The labeling reaction was quenched by the 200 mM Tris, pH 8.2 buffer, and the labeled protein was separated with a HiTrap desalting column into buffer containing 50 mM Tris, pH 8.0, 300 mM NaCl, and 4 mM β-ME. Fluorescence labeling efficiency was measured by Nanodrop 2000 (Thermo Fisher).

#### In vitro phase transition assay

All purified proteins were exchanged into the buffer containing 50 mM Tris, pH 8.0, 300 mM NaCl, and 4 mM β-ME. After centrifugation at 16,873 g for 10 min at 4°C, samples were placed on ice prior to the phase transition assay.

For sedimentation-based assays, GIT1 protein, GIT1/β-Pix mixture, or GIT1/β-Pix/Paxillin mixture each with total volume of 50 μL was incubated at room temperature for 10 min. Then, the mixture was centrifuged at 16,873 g for 3 min at 22°C. Samples from supernatant fraction and pellet fraction were analyzed by SDS-PAGE with Coomassie blue staining. Each assay was performed three times. The intensity of each band on SDS-PAGE was quantified by ImageJ and data were presented as mean ± SD.

For microscope-based assays, each sample was injected into a home-made chamber as described previously (Zeng et al., 2016) for DIC (Nikon eclipse 80i) or fluorescent imaging (Zeiss LSM 880).

#### Fluorescence recovery after photo-bleaching assay

FRAP assay was performed on a Zeiss LSM 880 confocal microscope with a 40X oil objective. For *in vitro* FRAP experiments on fluorophore labeled proteins, Cy3 signal was bleached by 561 nm laser beam at room temperature. For FRAP assay on puncta in living cell, HeLa cells were cultured on glass-bottom dishes (MatTek) and transfected with the indicated plasmids. GFP signal was bleached with 488 nm laser beam at 37°C.

For each experiment, the fluorescence intensities of a neighboring droplet with similar size to the bleached one were also recorded for intensity correction. Background was subtracted before data analysis. The ROI intensity at time 0 s (right after the photobleaching) was set as 0% and the pre-bleaching intensity was normalized to 100%.

#### HeLa cell imaging, focal adhesion localization and cell migration

HeLa cells were cultured on 12-well plates and transfected with the indicated plasmids using Viafect (Promega, Madison, WI). After expression for 24h, cells were fixed with 4% paraformaldehyde (PFA) and immunostained with the indicated antibodies. Images were acquired on Leica SP8 or Zeiss LSM 880 confocal microscope by a 40 × oil lens. Images were processed and analyzed using ImageJ. For focal adhesion localization analysis, three independent experiments were conducted in a blinded fashion. Focal adhesion regions were outlined and selected based on the Paxillin channel. The focal adhesion enrichment ratio was calculated as  $[\text{GFP}_{\text{FA}} \text{ intensity}] / [\text{GFP}_{\text{cytoplasm}} \text{ intensity}]$  or  $[\beta\text{-Pix}_{\text{FA}} \text{ intensity}] / [\beta\text{-Pix}_{\text{cytoplasm}} \text{ intensity}]$ , respectively.

Cell migration experiment was performed using Transwell membrane filter inserts (8 μm pore size, Corning costar).  $1 \times 10^5$  HeLa cells were seeded into the upper chamber and allowed to migrate into the lower chamber for 16-18h at 37°C. Cells in the upper chamber were carefully wiped by cotton buds, cells at the bottom of the membrane were washed once with PBS, and fixed by 100% methanol for 10 min, and then stained with Crystal Violet Staining Solution (Beyotime Biotechnology) for 10 min. The migrated cells were counted under a light microscope from five random fields of each well. All experiments were performed three times.

### Primary hippocampal neuron culture and imaging

Hippocampal neuron cultures were prepared as previously described (Zhu et al., 2017). At DIV14, neurons were transfected with 2 mg indicated plasmids per well (12-well plate) using Lipofectamine 2000 reagent (Invitrogen). Neurons were fixed at DIV18 with 4% paraformaldehyde (PFA) together with 4% sucrose in 1 × PBS buffer and mounted on slides for imaging. Confocal images were obtained using a Leica SP8 confocal microscope with a 40 × oil-immersion lens. Transfected neurons were chosen randomly for quantification from at least three independent batches of cultures. For detailed spine visualization, an additional 4 × zoom factor was applied. Normally, four randomly selected dendrites (~65 μm in length each) were imaged and analyzed from an individual neuron. Each image was collected as a z series maximum projection with 0.35-μm depth intervals. Intensity was measured with ImageJ.

### QUANTIFICATION AND STATISTICAL ANALYSIS

Statistical parameters including the definitions and exact values of n (e.g., number of experiments), distributions and deviations are reported in the Figures and corresponding Figure Legends. For focal adhesion localization and transwell migration assay, the results were expressed as mean ± SEM; ns, not significant, \*\*\*\*p < 0.0001, \*\*\*p < 0.001, \*\*p < 0.01, using one-way ANOVA with Dunnett's multiple comparison test. For synaptic targeting and spine development assay, the results were expressed as mean ± SEM; ns, not significant, \*\*p < 0.01, \*\*\*p < 0.001, \*\*\*\*p < 0.0001, using one-way ANOVA with Tukey's multiple comparison test. Statistical analysis was performed by GraphPad Prism.

**Molecular Cell, Volume 79**

**Supplemental Information**

**GIT/PIX Condensates Are Modular and Ideal  
for Distinct Compartmentalized Cell Signaling**

**Jinwei Zhu, Qingqing Zhou, Yitian Xia, Lin Lin, Jianchao Li, Mengjuan Peng, Rongguang Zhang, and Mingjie Zhang**

## Supplemental Information

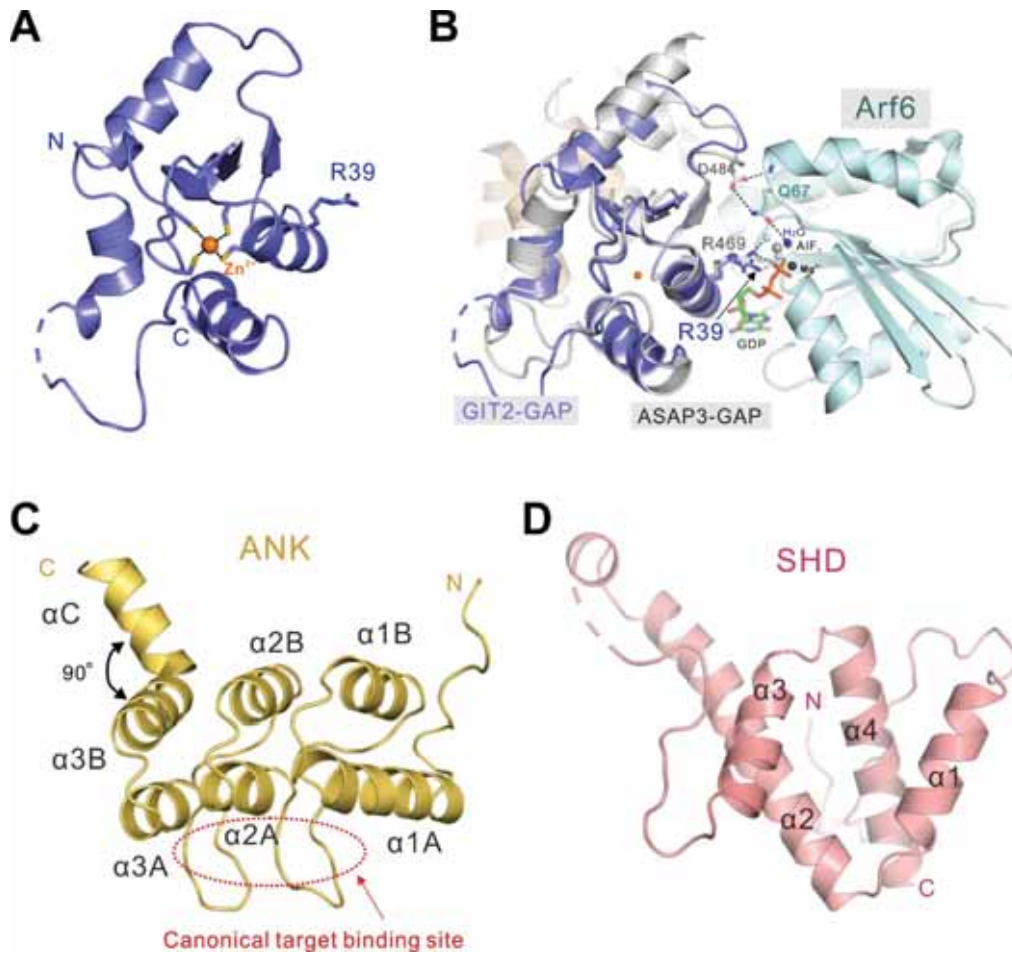


**Figure S1. Structural analysis of ArfGAP, ANK, and SHD domains of GIT2, Related to Figures 1&2.** (A) Ribbon diagram representation of the structure of ArfGAP domain. A zinc ion coordinated by four cysteines is shown. The arginine finger, R39, is shown in stick mode. (B) Superimposition of the structure of  $GAP^{GIT2}$  with that of  $GAP^{ASAP3}$  (PDB code: 3LVQ) showing that a conserved arginine of  $GAP^{GIT2}$ , R39<sup>GIT2</sup>, aligns well with the arginine finger of ASAP3, R469<sup>ASAP3</sup>, which is required for GTP hydrolysis. (C-D) Ribbon diagram representations of the structures of ANK (C) and SHD (D) domains.

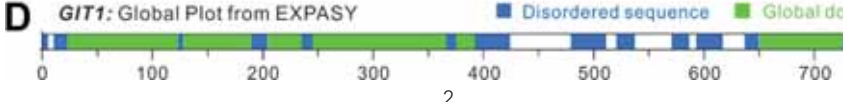
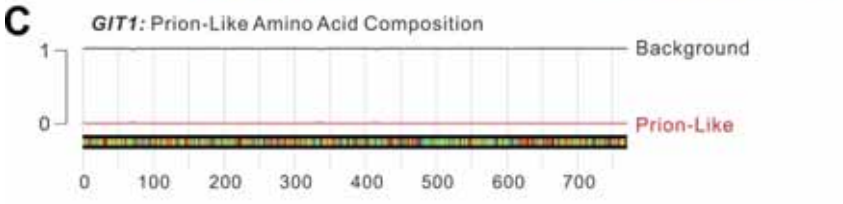


**Figure. S2 Sequence analysis of GIT and PIX family proteins, Related to Figures 1-3. (A)** Structure-based sequence alignment of GIT family proteins. In this alignment, the identical residues are highlighted with red boxes, and the conserved residues are color in red. Residues required for domain-domain coupling in GIT GAS tandem and PIX-GBD binding are indicated by black and blue dots, respectively. **(B)** Sequence alignment of GBD domains of PIX family proteins. The identical residues are color in red. Residues required for GIT GAS binding are indicated by blue dots. **(C-D)** Sequence analysis of GIT1 using an online Prion-like Amino Acid Composition prediction tool (PLAAC, <http://plaac.wi.mit.edu/>) **(C)** and the Global Plot tool (<http://globplot.embl.de/>) from EXPASY **(D)**, showing that GIT1 does not have prion-like sequence and the predicted disordered sequences are relatively short and discontinuous.

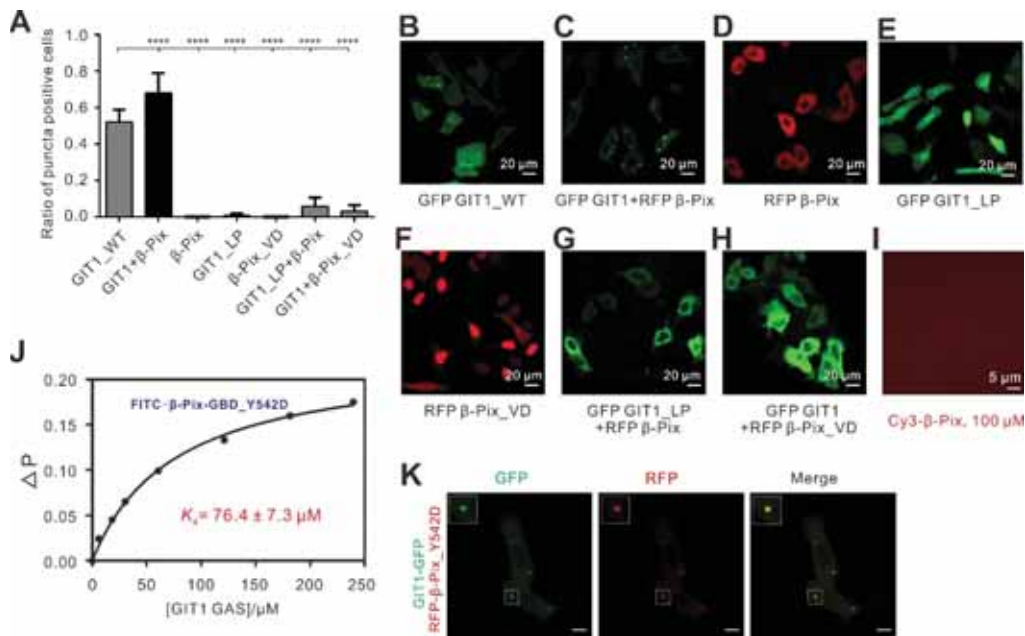


**Figure S3. Analysis of phase separated droplets in the cytoplasm formed by various forms of GIT and/or  $\beta$ -Pix, Related to Figures 3&4.** (A) Quantification results showing the fraction of puncta positive cells expressing various forms of GIT and/or  $\beta$ -Pix. The data were derived from 3 batches of cultured HeLa cells and shown as means  $\pm$ SDs, with the total cell number  $n > 200$  for each condition. Each group was compared to the GIT1\_WT using One-way ANOVA with Dunnett's multiple comparison test. ns, not significant; \*\* $p < 0.01$ ; \*\*\* $p < 0.001$ ; \*\*\*\* $p < 0.0001$ . (B-H) Representative images of HeLa cells expressing GFP-tagged GIT (GIT1\_WT-GFP, GIT1\_LP-GFP) and RFP-tagged PIX ( $\beta$ -PIX,  $\beta$ -PIX\_VD) plasmids as indicated. Note that neither GIT\_LP nor PIX\_VD mutant could form phase separated droplets in living cells. (I)  $\beta$ -Pix alone could not form phase separation at the concentration of 100  $\mu\text{M}$ . (J) Fluorescence polarization assay showing that the  $\beta$ -Pix-GBD\_Y542D mutant bound with GIT1 GAS with a  $K_d$  of  $\sim 76.4 \mu\text{M}$ . (K) Representative images showing that co-expression of GIT1-GFP and RFP- $\beta$ -Pix\_Y542D in HeLa cells produced multiple spherical puncta. Scale bars in Panels B-H are indicated in each image. Scale bar for Panel K: 5  $\mu\text{m}$ .

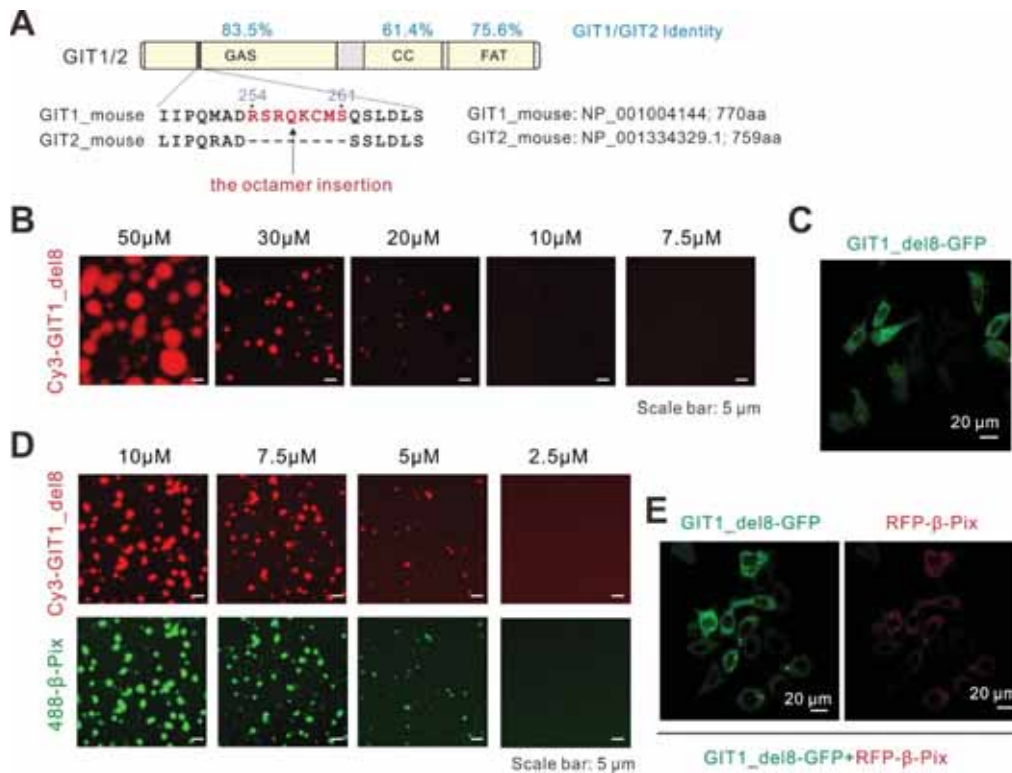


**Figure S4. GIT1<sub>del8</sub> and WT GIT1 displayed the same phase separation property in vitro and in heterologous cells, Related to Figures 3 and 4.** (A) Sequence analysis of GIT1 and GIT2. The sequence identities of the three domains between the two proteins are indicated. An 8-residue insert unique in GIT1 GAS tandem is highlighted in red. (B-C) GIT1<sub>del8</sub> could form phase separated droplets in vitro and in living cells. (D-E) GIT1<sub>del8</sub>/β-PIX form phase separated droplets in vitro and in living cells.

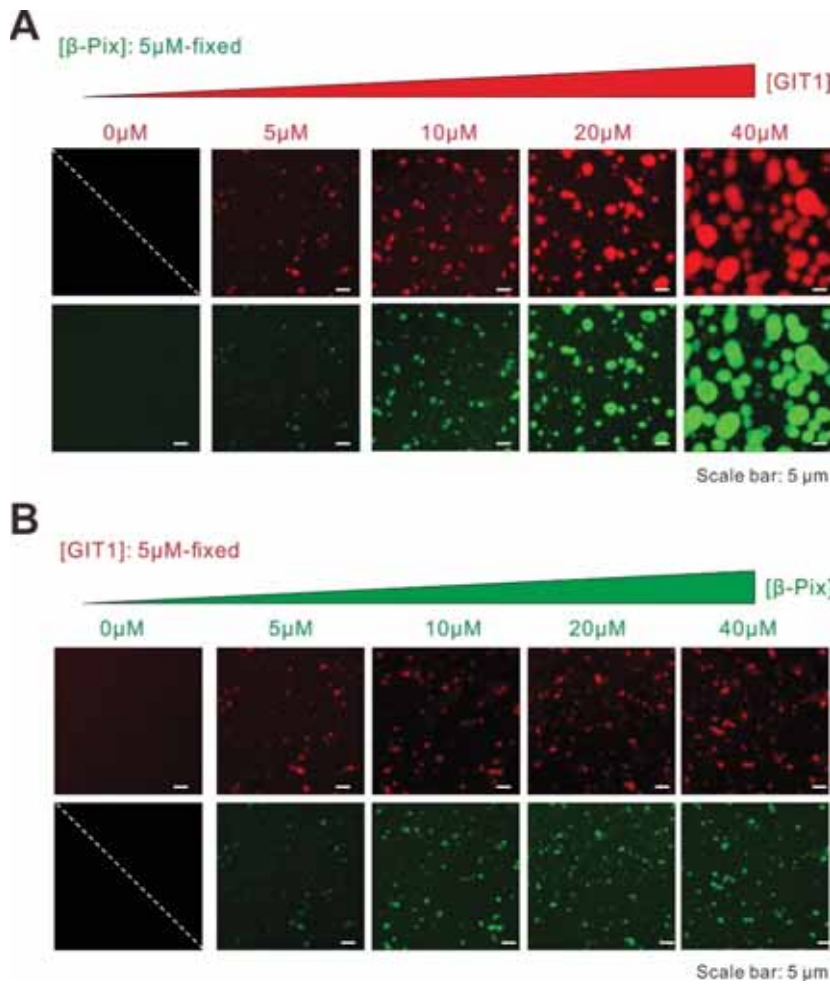


**Figure S5. Phase diagram of the GIT1/β-Pix condensates, Related to Figure 4. (A)** The concentration of β-Pix was fixed at 5 μM and increased amount of GIT1 (from 0 to 40 μM) was gradually added into β-Pix. When GIT1 and β-Pix were at 1:1 molar ratio, they formed liquid-like droplets. The size of droplets increased when the molar ratio of GIT1/β-Pix increased. **(B)** When the concentration of GIT1 was fixed at 5 μM and gradually increasing the amount of β-Pix (from 0 to 40 μM), the GIT1/β-Pix co-condensates appeared at 1:1 molar ratio and more or less saturated when β-Pix was in slight excess. Scale bar: 5 μm.

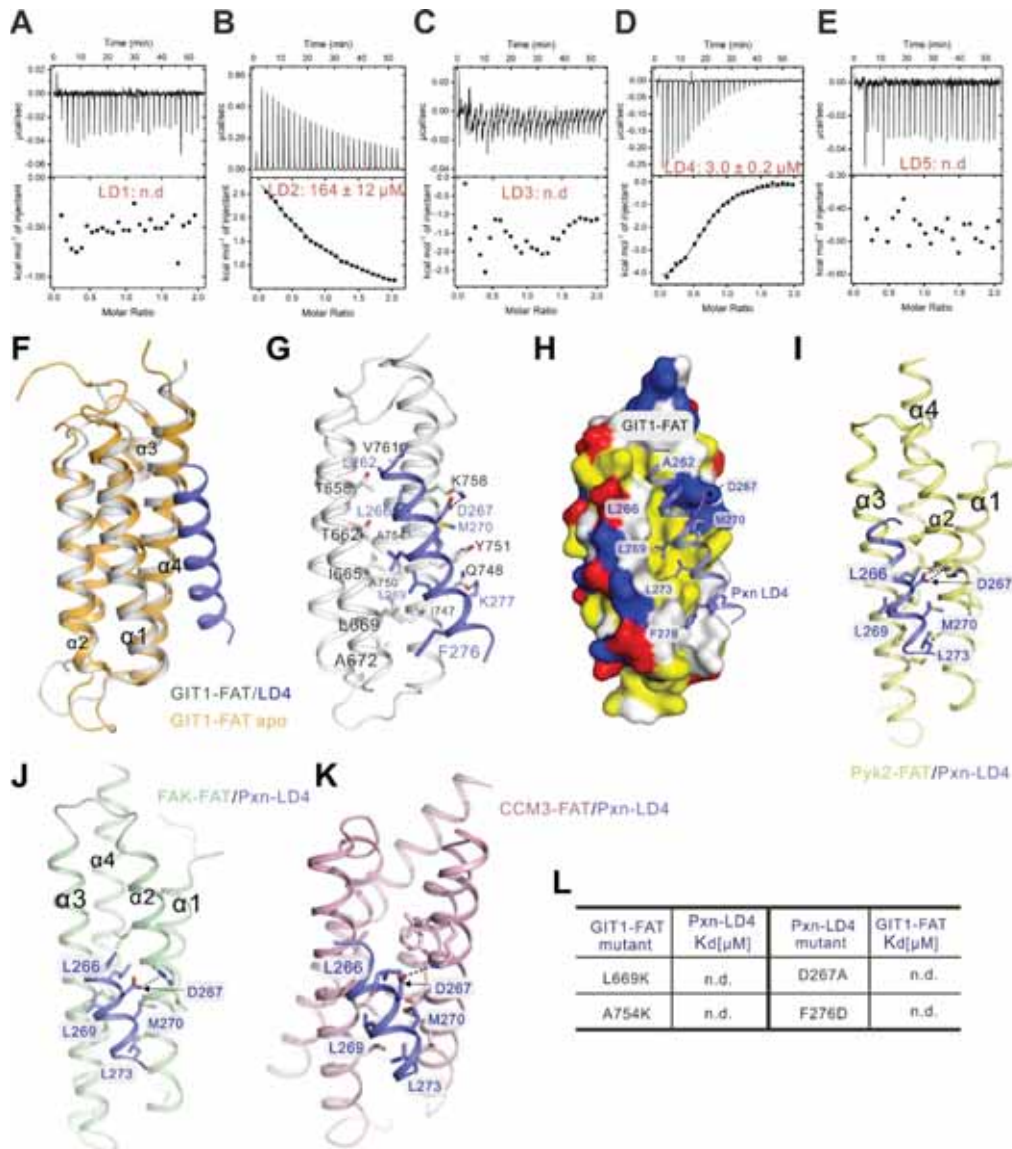


**Figure S6. Biochemical and structural study of GIT1/Paxillin interaction, Related to Figure 5. (A-E)** ITC titration curves showing the bindings of Paxillin LD motifs to GIT1-FAT. ITC-based binding curves of LD1 (A), LD2 (B), LD3 (C), LD4 (D), LD5 (E) to GIT1-FAT. **(F)** Superimposition of the structures of the GIT1 FAT/Paxillin LD4 complex and apo GIT1 FAT. **(G)** Detailed interactions between GIT1 FAT and Paxillin LD4. **(H)** The combined surface and ribbon representations of the GIT1 FAT/Paxillin LD4 interface showing that the binding is mainly mediated by hydrophobic interactions. **(I-K)** Structures of Pky2 FAT/LD4 (PDB code: 4R32) (I), FAK FAT/LD4 (PDB code: 1OW6) (J), CCM3 FAT/LD4 (PDB code: 3RQG) (K). **(L)** ITC-based assays showing that mutations of selected key residues involved in the GIT1 FAT/Paxillin LD4 interface abolished the complex formation. n.d., not detectable.

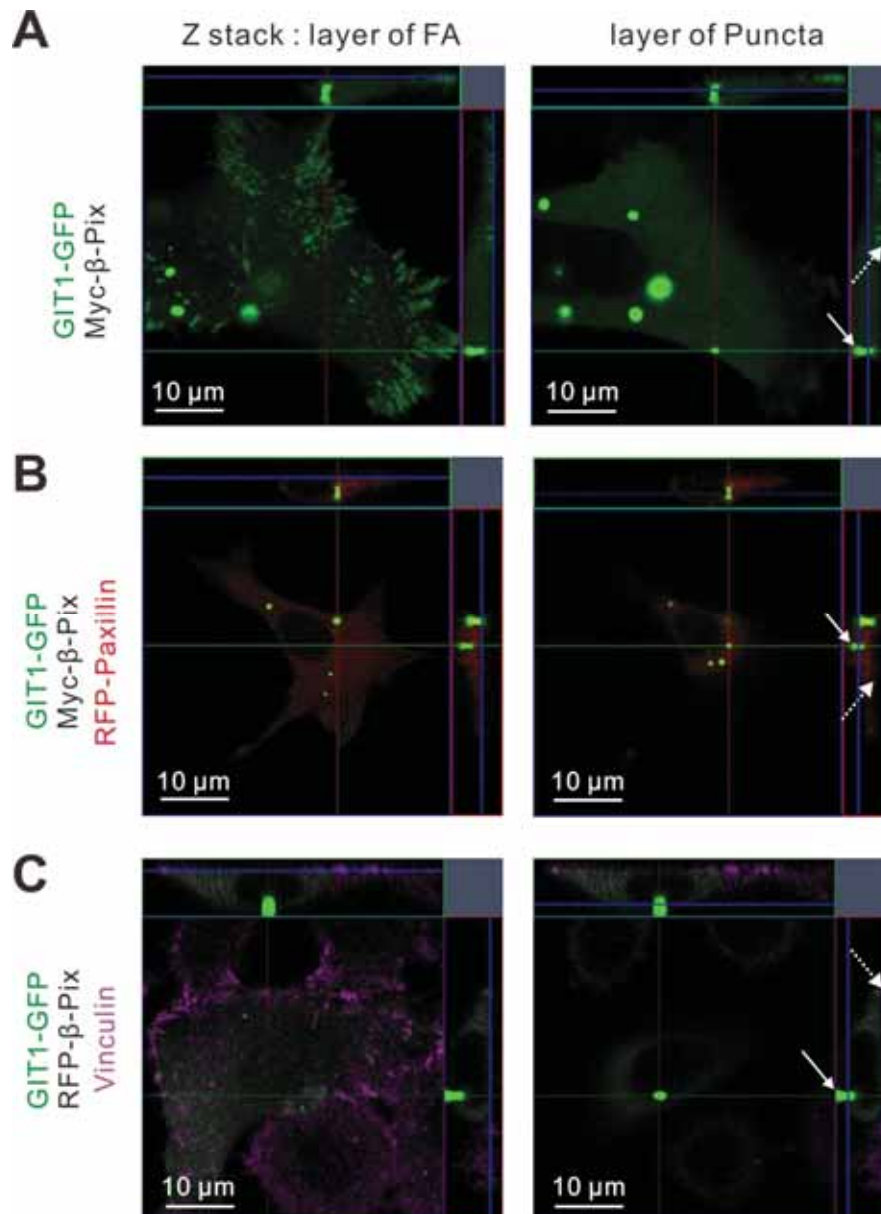


**Figure S7. Z stack image analysis of GIT1-mediated phase separations in HeLa cells, Related to Figures 3&4.** (A) When GIT1-GFP was co-expressed with Myc- $\beta$ -Pix, the GIT1/ $\beta$ -Pix condensates (white arrow) and FA-located GIT1 (white dashed arrow) were not in the same layer based on the Z stack analysis. (B) Similar findings were observed when GIT1-GFP, Myc- $\beta$ -Pix and RFP-Paxillin were co-expressed in HeLa cells. (C) the GIT1/ $\beta$ -Pix droplets (white arrow) were not in the same layer where endogenous vinculin resided (white dashed arrow).

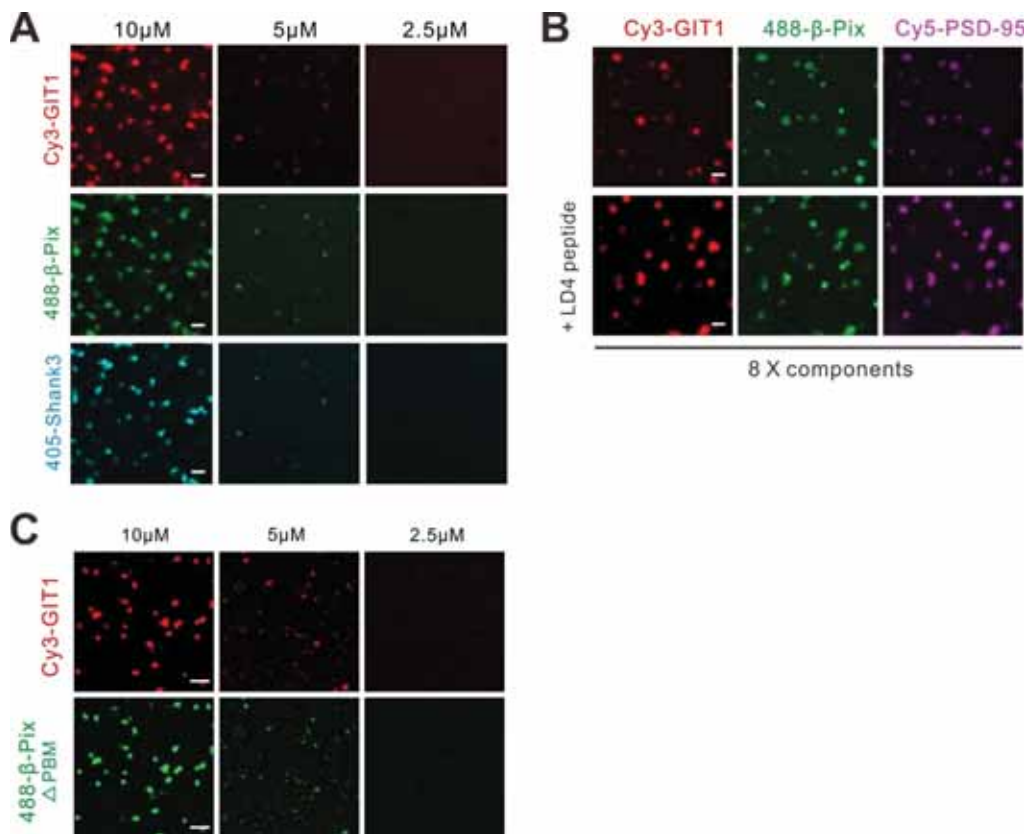


**Figure S8. Relationship between the GIT1-mediated condensates and the PSD condensate, Related to Figure 6.** (A) Fluorescence images showing that mixing GIT1,  $\beta$ -Pix and Shank3 at indicated concentrations resulted in condensed droplets with three proteins simultaneously enriched in the condensed phase. Shank3, GIT1 and  $\beta$ -Pix were labeled with iFluor405, Cy3 and Alexa488, respectively, with each at 1% level. Scale bar: 5  $\mu$ m. (B) Fluorescence images showing that addition of the LD4 peptide (200  $\mu$ M) into the mixture of GIT1 and  $\beta$ -Pix (both proteins are in their full-length forms and each at the concentration of 5  $\mu$ M) did not affect the phase separation of the two proteins. GIT1 and  $\beta$ -Pix were labeled with Cy3 and Alexa488 at 1%, respectively. Scale bar: 5  $\mu$ m. (C) Fluorescence images showing that mixture of GIT1 and  $\beta$ -Pix $^{\Delta$ PBM led to phase separation at indicated concentrations. GIT1 and  $\beta$ -Pix $^{\Delta$ PBM were labeled with Cy3 and Alexa488 at 1%, respectively. Scale bar: 10  $\mu$ m.

**Table S1. Data collection and refinement statistics, Related to Figures 1&2**

<b>Data collection and processing</b>		
Dataset	GIT2/ $\beta$ -Pix	GIT1/paxillin
Source	SSRF-BL19U1	SSRF-BL19U1
Wavelength( $\text{\AA}$ )	0.97775	0.97853
Space group	P2 <sub>1</sub> 2 <sub>1</sub> 2	P2 <sub>1</sub>
Unit cell(a,b,c, $\text{\AA}$ )	169.0, 322.7, 44.5	31.2, 91.0, 52.3
Unit cell( $\alpha,\beta,\gamma$ , $^\circ$ )	90,90,90	90, 107.4, 90
Resolution range ( $\text{\AA}$ )	50.00-2.80 (2.85-2.80)	50.00-2.00 (2.03-2.00)
No. of unique reflections	59001 (2912)	18573 (904)
Redundancy	8.1 (7.7)	6.8 (6.8)
I/ $\sigma$ (I)	11.8 (3.0)	16.0 (2.3)
Completeness (%)	95.8 (97.6)	98.6 (98.8)
R <sub>merge</sub> (%) <sup>a</sup>	17.5 (76.0)	11.4 (76.4)
<b>Structure refinement</b>		
Resolution ( $\text{\AA}$ )	44.05-2.80 (2.84-2.80)	45.48-2.00 (2.10-2.00)
R <sub>work</sub> <sup>b</sup> /R <sub>free</sub> <sup>c</sup> (%)	19.41 (25.99)/25.36 (31.43)	17.28 (23.42)/20.39 (25.82)
rmsd bonds ( $\text{\AA}$ )/angles ( $^\circ$ )	0.009/1.184	0.008/1.063
Number of reflections		
Working set	55585 (2301)	17567 (2493)
Test set	2987 (147)	970 (158)
Number of protein atoms	16305	2290
Number of solvent atoms	0	212
Average B factor ( $\text{\AA}^2$ )	45.2	32.9
Ramachandran plot(%)		
Most favored regions	97.4	97.2
Additionally allowed	2.6	2.8
Generously allowed	0	0

Numbers in parentheses represent the value for the highest resolution shell.

<sup>a</sup> R<sub>merge</sub> =  $\sum |I_i - I_m| / \sum I_i$ , where  $I_i$  is the intensity of the measured reflection and  $I_m$  is the mean intensity of all symmetry related reflections.

<sup>b</sup> R<sub>cryst</sub> =  $\sum ||F_{obs}| - |F_{calc}|| / \sum |F_{obs}|$ , where  $F_{obs}$  and  $F_{calc}$  are observed and calculated structure factors.

<sup>c</sup> R<sub>free</sub> =  $\sum T ||F_{obs}| - |F_{calc}|| / \sum T |F_{obs}|$ , where T is a test data set of about 5% of the total reflections randomly chosen and set aside prior to refinement.